이학박사학위논문

Generating and Quantifying Macroscopic Quantum States of Atomic and Optical Systems

원자계와 광학계에서의 거시 양자 상태 생성과 정량화

2015년 2월

서울대학교 대학원
물리·천문학부
강 민 수

Generating and Quantifying Macroscopic Quantum States of Atomic and Optical Systems

Minsu Kang

Supervised by

Associate Professor **Hyunseok Jeong**

A Dissertation
Submitted to the Faculty of
Seoul National University
in Partial Fulfillment of
the Requirements for the Degree of
Doctor of Philosophy

February 2015

Department of Physics and Astronomy
Graduate School
Seoul National University

Abstract

Generating and Quantifying Macroscopic Quantum States of Atomic and Optical Systems

Minsu Kang
Department of Physics and Astronomy
The Graduate School
Seoul National University

We discuss a classification of quantum effects based on possibility of emergence in macroscopic scales. We regard a certain phenomena as a genuine macroscopic quantum effect, if it cannot be described by any classical physics nor an accumulation of microscopic quantum effects. A quantum state corresponding to such effect is called a macroscopic quantum state.

One prominent aspect among various quantum effects is quantum entanglement. We investigate possibilities of generating macroscopic entanglement between an atom and a thermal state or even between multiple thermal states. We found entanglement is always risen for an arbitrarily large temperature of the thermal states. This indicates importance of coherent interactions rather than the necessity of initial purities.

We also propose a generation scheme for hybrid entanglement, which is comprised of classical and quantum states, based on single–photon addition technique. The key idea is that adding a single photon into a coherent state makes another approximate coherent state with a larger amplitude. Since it does not require in–line nonlinear interactions, it is experimentally feasible compared to traditional schemes.

Besides generating entanglement, we also attempt to quantify the macroscopic quantumness for arbitrary quantum states of spins. We construct a measure of macroscopic quantumness by counting oscillations of interference fringes in phase space. We apply the measure to typical and intuitive macroscopic quantum states and verify that the measure works properly. Remarkably, we show that quantum phase transition is a naturally occurring genuine macroscopic quantum effect in the spirit of Schrödinger's cat.

Keywords : Macroscopic quantum states, Atomic systems, Optical systems
Student Number : 2009-20391

Contents

List of Figures

Chapter 1

Introduction

Quantum physics has been successful to describe and predict behaviors of microscopic objects like atoms and photons. One of the critical characteristic of quantum mechanics is superposition, which implies any linear sum of two different physically valid states is also another valid physical state [1]. For instance, two different state of a spin–half particle, up *or* down, can be in a superposed state that can be said the spin is up *and* down at the same time. Among the pioneers of quantum physics, Erwin Schrödinger argued [2] that if quantum physics is universally valid, macroscopically distinguishable states like being alive *or* dead of a cat can be in a superposition turned being alive *and* dead, at the same time. However, as macroscopic lives, we never observe such a counter–intuitive state of a cat and it is even difficult to imagine of them. Instead of regarding an intractable real cat, many experimentalist have attempted to generate such superpositions of macroscopically distinct states in atomic/molecular systems [3, 4], superconducting circuits [5, 6], optical systems [7, 8, 9, 10, 11], and mechanical systems [12]. If macroscopic superposition is comprised of a multiple number of parties, they are also seen as macroscopic entanglement. There are different types

of macroscopic entanglement, such as squeezed macroscopic entanglement [13, 14, 15, 16, 17, 18, 19], Greenberger-Horne-Zeilinger type entanglement [20, 21, 22, 23], and so–called NOON states [24, 25, 26, 27]. However, whether such superpositions or quantum effects are completely coincide with the Schrödinger's argument is not apparent in both qualitative and quantitative manner. For instance, whether displaced vacuum and single photon states [28, 29] are macroscopically distinct is still an arguable issue.

In this thesis, we try to clarify the concepts of quantum effects and classify them into a certain hierarchy. We also propose several generation ideas of macroscopic superpositions for atomic and optical systems. Then we attempt to quantify the degree of macroscopic quantumness for spin systems. The quantification is based on the idea that was introduced for a optical system [30], however translating the idea into a different physical system is not straightforward. The contents are organized as follows. In Chapter 2, we classify several quantum effects into three categories; microscopic quantum effects, accumulation of microscopic quantum effects, and genuine macroscopic quantum effects. In Chapter 3, 4, we study entanglement generation schemes for atomic and optical states. In Chapter 5, we review an interference based measure of macroscopic quantumness for optical system and propose a measure for spin systems. Then we apply to various macroscopic quantum states and discuss about quantum phase transition. We conclude with final remarks in Chapter 6.

Chapter 2

Macroscopic Quantum Effects

2.1 Accumulation of microscopic quantum effects

There are well–known quantum effects that can be observed even in macroscopic scaled bulk materials. The very first of them is Plank's law in blackbody radiation which regards quantization of energy of light fields [31, 33]. Such discretization of energy has no counterpart of classical physics, which make it an apparent quantum effect by definition. However, we do not consider Plank's law as a same category of quantum effects that Schrödinger's cat implies, a *macroscopic quantum effect*. That is because Plank's law is about quantum effect of each individual light mode. The entire blackbody radiation spectrum can be explained by independent descriptions of each different light mode. As more developed examples, suppose superconductivity and superfluidity in bulk materials as well. Both of them are also obvious quantum effects where any classical models cannot predict [34]. However, in similar to the blackbody radiation, it is not required to describe entire constituting particles to explain such phenomena. For instance, a quantum state of

two electrons called the Cooper pair,

$$|\psi_{CP}\rangle = \frac{1}{\sqrt{2}} \left(|\uparrow\rangle |\uparrow\rangle + e^{i\phi} |\downarrow\rangle |\downarrow\rangle \right), \tag{2.1}$$

can explain passage of the two electrons through metallic lattice without resistance [32]. Thus the superconductivity of any large number of N electrons are explained accumulation of $N/2$ Cooper pairs $|\psi_{CP}\rangle^{\otimes N/2}$, which is not qualitatively different to the simple two electron case. In that sense, superconductivity is an *accumulation of microscopic quantum effects* [33, 34].

2.2 Genuine macroscopic quantum effects

There is another class of quantum effects emerging even in macroscopic scale yet cannot be explained by an accumulation of microscopic quantum effects. We refer such phenomena as a *genuine macroscopic quantum effect* since they are indeed not classical, nor cumulative microscopic quantum. One such effect recently acquiring its prominence is quantum metrology or also called quantum phase estimation [35, 36]. It is estimating an unknown parameter that a physical system under interest might possess. A typical setting of such scheme is Mach–Zehnder type of interferometers, where a probing state undergoes an evolution caused by a target element, and then be measured to obtain the information of the unknown parameter , say ϕ, acquired during the interaction [37] According to classical physics, its estimation precision limit is inversely proportional to the square root of a size of the probing

state N at most [38, 39],

$$\delta\phi \geq \frac{1}{\sqrt{N}}. \tag{2.2}$$

Such an inherent bound is called the standard quantum limit. However, if we utilize a well–engineered quantum superposition of a probing state, the boundary can be lowered beyond the classical limit, up to Heisenberg limit, which is inversely proportional to the size of the probing state [38, 39],

$$\delta\phi \geq \frac{1}{N}. \tag{2.3}$$

The improvement of the measurement precision originates in non–classical correlations between different degrees of the probing state. Since the entire particle is concurrently participating in such improvement, one cannot observe the same effect with discarding any single one of the particles. A loss of a single particle yields a loss of correlation or information that enables the probing state to become sensitive to the disturbance from the unknown element. In this sense, quantum phase estimation is a good example of a genuine macroscopic quantum effect which never can be explained or reproduced by a subset of the quantum system [33]. The quantum correlation causing such effects are traditionally though as quantum entanglement, of which detail is discussed in the next chapter. However, a proper degree of macroscopic quantumness does not perfectly overlaps with entanglement. We discuss this issue in Chapt. 5 and devise a measure of macroscopic quantumness for spins.

Chapter 3

Generating Entanglement from High Temperature Thermal States

3.1 Quantum entanglement

Quantum entanglement is a kind of correlation between more than two groups of physical systems that never can be described by any classical physics. Its concept first appears in Einstein–Podolsky–Rosen (EPR) paradox [40]. Suppose a quantum state of two spin–half particles,

$$\frac{1}{\sqrt{2}}\left(|\uparrow\rangle\,|\downarrow\rangle - |\downarrow\rangle\,|\uparrow\rangle\right). \tag{3.1}$$

It has a perfect correlation on measurement of z–directional spin measurement. If the first spin is measured as up, then the second one is down. Conversely, if the first is down then the second is up. However, one can generate such a correlation in a classical manner as well using classical statistics. What makes this state non–classical is that the perfect correlation always happens regardless of the measurement basis. We can rewrite the state in an arbitrary

spin–half basis as

$$\frac{1}{\sqrt{2}}\left(|\uparrow_{\theta,\phi}\rangle\,|\downarrow_{\theta,\phi}\rangle - |\downarrow_{\theta,\phi}\rangle\,|\uparrow_{\theta,\phi}\rangle\right), \tag{3.2}$$

where $|\uparrow_{\theta,\phi}\rangle = \cos\theta\,|\uparrow\rangle + \sin\theta e^{i\phi}\,|\downarrow\rangle$ with an arbitrary angles θ and ϕ. The opposite basis is then found as $|\downarrow_{\theta,\phi}\rangle = \sin\theta\,|\uparrow\rangle - \cos\theta e^{i\phi}\,|\downarrow\rangle$ so that the orthogonality is satisfied, $\langle\uparrow_{\theta,\phi}\mid\downarrow_{\theta,\phi}\rangle = 0$.

We can clarify a strict definition of entanglement in terms of mathematical forms of quantum states. For an arbitrary bipartite pure state $|\psi_{AB}\rangle$, the two parties are entangled if it cannot be written as a product form of local quantum states as [41]

$$|\psi_{AB}\rangle \neq |\psi_A\rangle \otimes |\psi_B\rangle \tag{3.3}$$

for any possible local basis. More generally, for a bipartite mixed state ρ_{AB}, it is entangled if it cannot be written as a convex sum of product states [42] as

$$\rho_{AB} \neq \sum_i p_i \rho_A^i \otimes \rho_B^i. \tag{3.4}$$

The numerical value of entanglement can be measured by negativity of partial transpose (NPT) [43, 44, 45], which is defined as

$$-\,2\min(0,\epsilon), \tag{3.5}$$

where ϵ is the minimum eigenvalue of the partial transpose of the density matrix with respect to one of its parties. A mathematical reason that it captures the entanglement is that a density matrix with the condition Eq. (3.4) does not preserve the positivity under the partial transposition bearing negative eigenvalues [43].

3.2 Thermal states

The strict definition of a thermal state is a quantum description of a light field radiated from a blackbody following the Plank's law, which implies the distribution of spectral radiances over all possible frequencies. However, for a specific purpose, where the atomic frequency is resonant with the light field, we define a restricted meaning of a thermal state as one that follows Boltzmann distribution with a single frequency,

$$\rho^{th}(\lambda) = (1-\lambda)\sum_{n} \lambda^n \left|n\right\rangle\!\left\langle n\right|, \tag{3.6}$$

where $|n\rangle$ is the n–photon number state of light. A parameter determining the temperature is given as $\lambda = \exp[-\hbar\omega/k_B T]$, where k_B is the Boltzman constant, ω is the frequency of the optical field. For the limit of zero–temperature ($T \to 0$) the thermal state becomes a vacuum $|0\rangle$. If the temperature goes to infinity, the thermal state is a complete mixture of all possible photon number states. The thermal state is regarded a classical state since it has no quantum coherence among each photon number states. Furthermore, it can be macro-

scopic for a large enough temperature to contain a macroscopic number of photons that can be detected even by naked human eyes. In mathematical terms, it is a steady state solution (*i.e.* $d\rho/dt = 0$) for the following master equation

$$\frac{d\rho}{dt} = -\frac{i}{\hbar}[\hbar\omega, \hat{a}^\dagger\hat{a}] + \frac{\gamma}{2}(\bar{n}+1)(2\hat{a}\rho\hat{a}^\dagger - \hat{a}^\dagger\hat{a}\rho - \rho\hat{a}^\dagger\hat{a}) + \frac{\gamma}{2}\bar{n}(2\hat{a}^\dagger\rho\hat{a} - \hat{a}\hat{a}^\dagger\rho - \rho\hat{a}\hat{a}^\dagger), \tag{3.7}$$

where γ is the decay rate due to coupling to external reservoirs and $\bar{n}$ is the average photon number in the thermal bath. The first term of Eq. (3.7) describes the evolution due to self energy and the second term is losing excitation and the last term is acquiring excitation. Therefore, the thermal state does not suffer from decoherence at all.

The thermal state also can be represented in terms of coherent state basis. For the later purpose, we additionally act a displacement operation, $D(d)\,|\alpha\rangle \propto |\alpha + d\rangle$, to the original thermal state and it is represented as

$$\rho^{th}(V, d) = \int d^2\alpha P^{th}_\alpha(V, d)|\alpha\rangle\langle\alpha|, \tag{3.8}$$

where

$$P^{th}_\alpha(V, d) = \frac{2}{\pi(V-1)} e^{-\frac{2|\alpha-d|^2}{V-1}} \tag{3.9}$$

is the Glauber–Sudarshan P–representation [46], and $|\alpha\rangle$is a coherent state of amplitude α. The variance V is related to the average photon number $\bar{n}$

as $V = 2(\bar{n} - d^2) + 1$. Note that $P_\alpha^{th}(V, d)$ is completely positive for any α and d. Since the displacement is unitary, it does not change the purity $\mathrm{Tr}[(\rho^{th})^2] = V^{-1}$ of the thermal state.

3.3 Entanglement of thermal states

In general, generating entanglement using a classical state is much more difficult than using a nonclassical state. For example, it was shown that nonclassicality is a prerequisite of generating entanglement of light fields using a beam splitter [47]. On the other hand, it is possible to generate entanglement with highly mixed thermal states under certain conditions [48, 49, 50, 51, 52, 53, 54]. Bose *et al.* showed [49] that entanglement always arises between a two-level atom and a thermal field inside a cavity irrespective of the temperature of the thermal state as far as the atom was initially in a pure excited state. In their work, the Jaynes-Cummings (JC) interaction was used to model the cavity interaction. This indicates that the purity of the atom enforces the atom and the thermal state to become entangled even when the thermal state is extremely mixed. Kim *et al.* showed [50] that two atoms can become entangled through their interactions with a thermal field when the two atoms are initially in their pure states. Jeong and Ralph also pointed out [52] that entanglement between thermal states at arbitrarily high temperatures can be generated using a cross-Kerr nonlinear interaction if an ancillary microscopic superposition is used with a conditioning measurement.

However, we can further generalize the problems. For example, it would be another interesting question whether a thermal state at an arbitrarily high temperature can ever be entangled with a mixed atomic state by a direct unitary interaction. It also remains unanswered whether entanglement may be generated between thermal states at arbitrarily high temperatures by a direct unitary interaction. In this chapter, we study several examples to answer these questions. We conclude that entanglement between two thermal states can be generated solely by a unitary interaction even when both the states have purities arbitrarily close to zero. Our results show that subsystem purity, at any degree, is not a necessary condition for generating entanglement by a direct unitary interaction. Thus the importance of the initial purity depends on the interaction model.

3.3.1 Entangling microscopic system and thermal state

Reference [49] shows that entanglement is always generated from a pure excited atom and a thermal field through a JC interaction irrespective of the temperature of the field. If both the atomic state and the cavity field are in thermal states with a same temperature, entanglement disappears in the infinite temperature limit [49]. The reason for this is that the total state becomes proportional to the identity as the temperature goes to infinity [49]. However, it is possible to prepare the initial atomic state in an independent manner from the temperature of the field. We here examine such examples where both parties are in mixed states but their degrees of purities are independently varied.

We consider an atomic state

$$p\,|e\rangle\langle e| + (1-p)\,|g\rangle\langle g| \tag{3.10}$$

with $0 \leq p \leq 1$, and a thermal-field state, ρ^{th} (Eq. (3.6)), where $|g\rangle$ ($|e\rangle$) is the ground (excited) state of the atom and $|n\rangle$ is the photon number state of the field. We also note that $\lambda = \exp[-\hbar\omega/k_BT]$, k_B is the Boltzman constant, T is the temperature, $\hbar$ is the Plank constant, and ω is the frequency of the optical field. In our analysis, the purity of state ρ is quantified by the linear entropy Tr$[\rho^2]$. The purities of the atomic and field states are then

$$\begin{aligned}\mathcal{P}_{\text{atom}} &= 2(p-\frac{1}{2})^2 + \frac{1}{2} \\ \mathcal{P}_{\text{field}} &= \frac{1-\lambda}{1+\lambda}\end{aligned} \tag{3.11}$$

, respectively. We take p and λ as independent control parameters of purities of the atom and the field. The purity of the atom is 1 when $p = 1$ while it shows the minimum value 1/2 when $p = 1/2$, and the purity of the field can be characterized by $0 \leq \lambda \leq 1$. The initial states evolve through a JC interaction

$$H_{\text{JC}} = g(|e\rangle\langle g|\,a + |g\rangle\langle e|\,\hat{a}^\dagger), \tag{3.12}$$

where g is the coupling strength and $\hat{a}$ ($\hat{a}^\dagger$) is the annihilation (creation) operator of the field mode. After the interaction with time t, we make a local

projection on the field mode into a subspace spanned by $|n\rangle$ and $|n+1\rangle$, then the total state becomes

$$p\begin{pmatrix} P_{n-1}S_{n-1}^2 & 0 & 0 & 0 \\ 0 & P_nC_n^2 & iP_nC_nS_n & 0 \\ 0 & -iP_nC_nS_n & P_nS_n^2 & 0 \\ 0 & 0 & 0 & P_{n+1}C_{n+1}^2 \end{pmatrix}$$
$$+q\begin{pmatrix} P_nC_{n-1}^2 & 0 & 0 & 0 \\ 0 & P_{n+1}S_{n+1}^2 & -iP_{n+1}C_nS_n & 0 \\ 0 & iP_{n+1}C_nS_n & P_{n+1}C_n^2 & 0 \\ 0 & 0 & 0 & P_{n+2}S_{n+1}^2 \end{pmatrix}, \qquad (3.13)$$

where

$$C_n = \cos\left(gt\sqrt{n+1}\right)$$
$$S_n = \sin\left(gt\sqrt{n+1}\right)$$
$$P_n = (1-\lambda)\lambda^n, \qquad (3.14)$$

and $q = 1 - p$. Since the projection is a local operation, observing nonzero NPT of the projected density matrix indicates that the original total state has entanglement.

A nonzero value of NPT for Eq. (3.13) with any value of n is an evidence of the atom-field entanglement. Values of the NPT for several choices of n

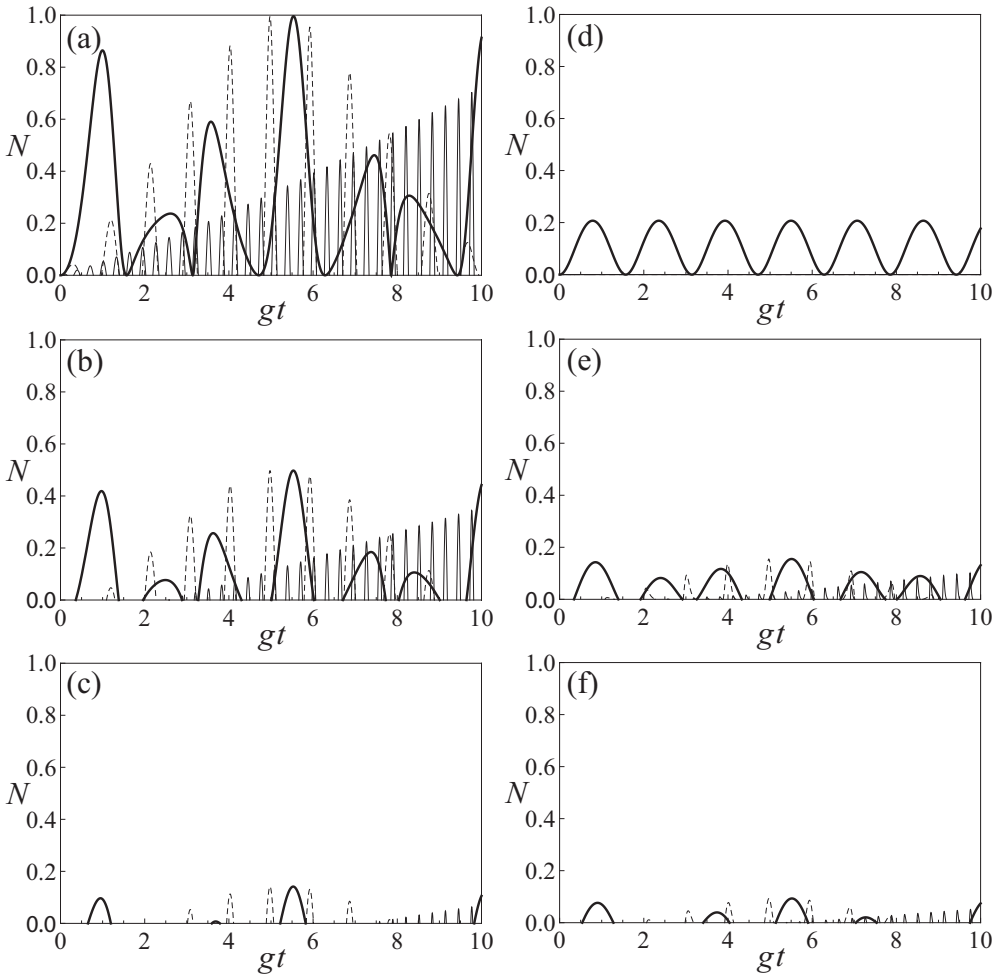

Fig. 1: The NPT of the projected density matrix versus (interaction strength)×(interaction time) for entanglement between an atom and a thermal state discussed in the main text. The projection basis on the field mode are $\{ |n\rangle\langle n|, |n+1\rangle\langle n+1|\}$ with $n = 0$ (thick), $n = 10$ (dashed), and $n = 100$ (thin). The temperature of the field is assumed to be infinite for (a-c) and purity p of the atomic state is (a) 1, (b) 0.9, and (c) 0.8. The atom is assumed to be maximally mixed ($p = 1/2$) for (d-f) and λ of the field is (d) 0, (e) 0.1, and (f) 0.2 in order of decreasing purity.

with normalizations of Eq. (3.13) are presented in Fig. 1. If the atom was initially in a pure excited state ($p = 1$), entanglement of the projected density matrix with $n = 0$ shows entanglement except when $gt = n\pi/2$. As shown in Fig. 1, the cases with the other projections ($n = 10$ and 100) of the density matrix lead to the conclusion that the entanglement always exists for $t > 0$. This is in agreement with the result of Ref. [49].

As shown in Fig. 1, the NPT tends to disappear as the purity of the atom decreases. In Fig. 1, we also observe similar behaviors when the initial atom is in a maximally mixed state $(|g\rangle\langle g| + |e\rangle\langle e|)/2$ and the temperature of the field increases from 0 to infinity. It seems that a certain degree of purity is required to generate entanglement. However, the method used here is merely to find a sufficient condition of the presence of entanglement, and we cannot confirm that there is no entanglement in the original state when the NPT is zero for the projected density matrix [49].

We consider an entanglement generation scheme between two harmonic oscillators studied in Refs. [52, 55]. It is analogous to the scheme in the previous section: the atomic state is replaced by a superposition of the vacuum and the single photon, and the JC interaction is replaced by a cross-Kerr nonlinear interaction. A limitation of the cross-Kerr interaction in implementing certain quantum gates has been pointed out [56]. However, we are here interested in possibility of entanglement generation using possible physical interactions in any systems. It is also worth noting [57] that a nonzero conditional phase shift with a high fidelity is possible in a cross-Kerr interaction between pulses

with unequal group velocities.

The cross-Kerr interaction between modes a and b is described by an interaction Hamiltonian

$$H_{\text{Kerr}} = \chi \hat{a}^\dagger \hat{a} \hat{b}^\dagger \hat{b}, \tag{3.15}$$

where χ is the nonlinear interaction strength. One mode is prepared as a superposition of the vacuum and the single photon state, generally in a mixture

$$\rho_{\text{m}} = \frac{1}{2}(|0\rangle\langle 0| + r|0\rangle\langle 1| + r|1\rangle\langle 0| + |1\rangle\langle 1|), \tag{3.16}$$

where the purity, Tr[ρ_{m}^2] = $(1 + r^2)/2$, is characterized by a real value r. One can see that Eq. (3.16) is a pure superposition $(|0\rangle + |1\rangle)/\sqrt{2}$ when $r = 1$. The other mode is prepared as a displaced thermal state, After a cross-Kerr interaction with an interaction time $t = \pi/\lambda$, the total state becomes

$$\begin{aligned} &\frac{1}{2}\big\{|0\rangle\langle 0| \otimes \rho^{th}(V, d) + |1\rangle\langle 1| \otimes \rho^{th}(V, -d) \\ &\quad + r|0\rangle\langle 1| \otimes \sigma(V, d) + r|1\rangle\langle 0| \otimes \sigma(V, -d)\big\}, \end{aligned} \tag{3.17}$$

where $\sigma(V, d) = \int d^2\alpha P_\alpha^{th} |\alpha\rangle\langle -\alpha|$. We make local projections on the total state into a subspace spanned by sets $\{|0\rangle, |1\rangle\}$ and $\{|+\rangle_\gamma, |-\rangle_\gamma\}$ where $|\pm\rangle_\gamma \equiv \mathcal{N}_\pm(|\gamma\rangle \pm |-\gamma\rangle)$ with $\mathcal{N}_\pm = 1/\sqrt{2(1 \pm \exp[-2\gamma^2])}$. The projected

state ρ_γ is then

$$\begin{pmatrix} \mathcal{N}_+^2 C_\gamma & \mathcal{N}_+\mathcal{N}_- S_\gamma & r\mathcal{N}_+^2 C_\gamma & -r\mathcal{N}_+\mathcal{N}_- S_\gamma \\ \mathcal{N}_+\mathcal{N}_- S_\gamma & \mathcal{N}_-^2 C_\gamma & r\mathcal{N}_+\mathcal{N}_- S_\gamma & -r\mathcal{N}_-^2 C_\gamma \\ r\mathcal{N}_+^2 C_\gamma & r\mathcal{N}_+\mathcal{N}_- S_\gamma & \mathcal{N}_+^2 C_\gamma & -\mathcal{N}_+\mathcal{N}_- S_\gamma \\ -r\mathcal{N}_+\mathcal{N}_- S_\gamma & -r\mathcal{N}_-^2 C_\gamma & -\mathcal{N}_+\mathcal{N}_- S_\gamma & \mathcal{N}_-^2 C_\gamma \end{pmatrix}$$
$$+ R_\gamma \begin{pmatrix} \mathcal{N}_+^2 & \mathcal{N}_+\mathcal{N}_- & r\mathcal{N}_+^2 & -r\mathcal{N}_+\mathcal{N}_- \\ \mathcal{N}_+\mathcal{N}_- & -\mathcal{N}_-^2 & -r\mathcal{N}_+\mathcal{N}_- & r\mathcal{N}_-^2 \\ r\mathcal{N}_+^2 & -r\mathcal{N}_+\mathcal{N}_- & \mathcal{N}_+^2 & \mathcal{N}_+\mathcal{N}_- \\ -r\mathcal{N}_+\mathcal{N}_- & r\mathcal{N}_-^2 & \mathcal{N}_+\mathcal{N}_- & -\mathcal{N}_-^2 \end{pmatrix}, \qquad (3.18)$$

where

$$\begin{aligned} C_\gamma &= \frac{4}{V+1}\text{exp}[-\frac{2}{V+1}(\gamma^2+d^2)]\text{cosh}[4\gamma d/(V+1)] \\ S_\gamma &= \frac{4}{V+1}\text{exp}[-\frac{2}{V+1}(\gamma^2+d^2)]\text{sinh}[4\gamma d/(V+1)] \\ R_\gamma &= \frac{4}{V+1}\text{exp}[-\frac{2}{V+1}(V\gamma^2+d^2)]. \end{aligned} \qquad (3.19)$$

We assumed that γ and d are real without loss of generality. Notice that $\text{Tr}[\rho_\gamma(r)] \neq 1$ because the local projection is not an unitary operation. The absolute scale of the NPT is not important for the purpose of our study, because any non-zero value is meaningful enough.

We numerically calculated the NPT of $\rho_\gamma(r)/\text{Tr}[\rho_\gamma(r)]$ for some values of V, d, and r, and present the results in Fig. 2. When $d = 0$, the NPT is

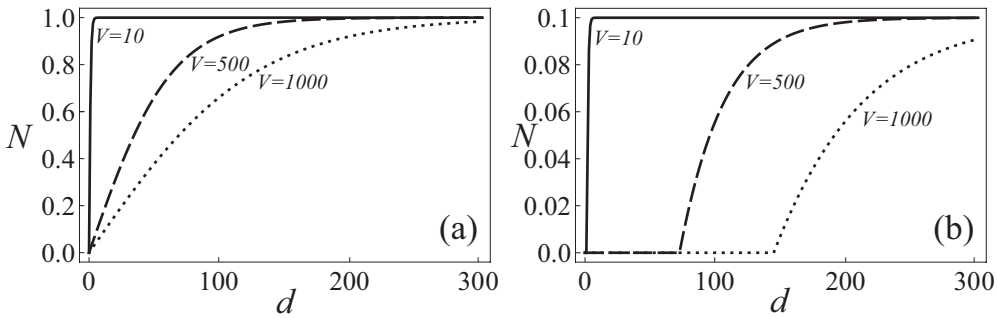

Fig. 2: The NPT of the projected density matrix for Eq. (3.18) against displacement d of the displaced thermal field. We choose amplitude $\gamma = 2$ for the projection basis $|\pm\rangle_\gamma$ with several values of V, and the normalized purity r is (a) 1 and (b) 0.1. Unless the microscopic superposition is totally mixed as $r = 0$, entanglement is observed for $d \gg \sqrt{V}$ for any values of V.

zero regardless of the value of V. In this case, the original state is separable because $\sigma(V,0)^T = \sigma(V,0)$ in Eq. (3.17): the density matrix is then invariant under a partial transpose on one side. However, we can observe entanglement for any values of V with $d \gg \sqrt{V}$ as far as r is nonzero in Eq. (3.16).

We now consider two slightly different entanglement generation schemes where conditioning measurements are used in addition to unitary interactions [52]. After the Kerr interaction between a microscopic state in Eq. (3.16) and a thermal state, we measure out the microscopic part on the basis $(|0\rangle \pm |1\rangle)/\sqrt{2}$ [52]. The resultant state of the remaining mode is highly non-classical exhibiting singular behaviors on its Wigner function [52]. After we transmit

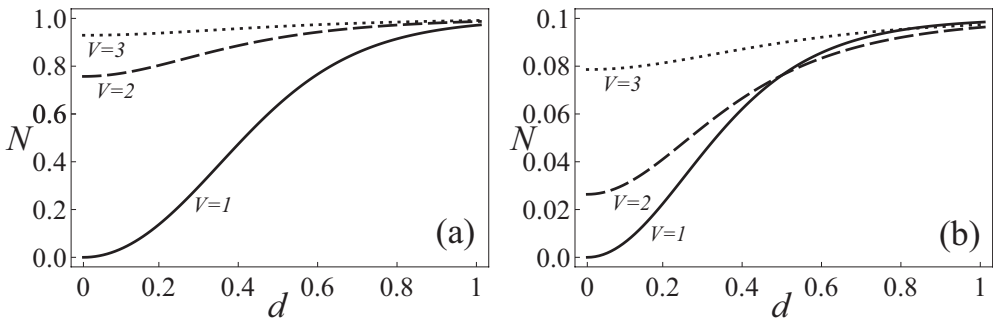

Fig. 3: The NPT of the locally projected state of $\rho^{BS(+)}$ with (a) $r = 1$ and (b) $r = 0.1$. We used $\gamma = 2$ for the projection basis. Entanglement is always observed for large values of $V \gg 1$ even when $d = 0$ unless $r = 0$.

this state through a 50:50 beam splitter, the state becomes

$$\begin{aligned}\rho^{BS(\pm)} =& N \int d^2\alpha P_\alpha^{th}(V,d)\big\{|\delta\rangle\langle\delta| \otimes |-\delta\rangle\langle-\delta| + |-\delta\rangle\langle-\delta| \\ & \otimes |\delta\rangle\langle\delta| \pm r|\delta\rangle\langle-\delta| \otimes |-\delta\rangle\langle\delta| \pm r|-\delta\rangle\langle\delta| \otimes |\delta\rangle\langle-\delta|\big\},\end{aligned} \tag{3.20}$$

where $\delta = \alpha/\sqrt{2}$ and $N = (2 \pm 2r\ \exp[-2d^2/V]/V)^{-1}$. The NPT of the locally projected density matrix by sets $\{|+\rangle_\gamma, |-\rangle_\gamma\}$ for both parties is plotted in Fig. 3. One can observe that entanglement between thermal states is generated even when they are highly mixed ($V \gg 1$) unless the initial microscopic state was totally mixed with $r = 0$. Interestingly, a high mixture ($V \gg 1$) enables one to observe entanglement even with $d = 0$ and a small value of r.

The other entanglement generation scheme between two macroscopic thermal states is as follows. The microscopic state successively interacts with two thermal states via the cross-Kerr interactions, and it is measured out along

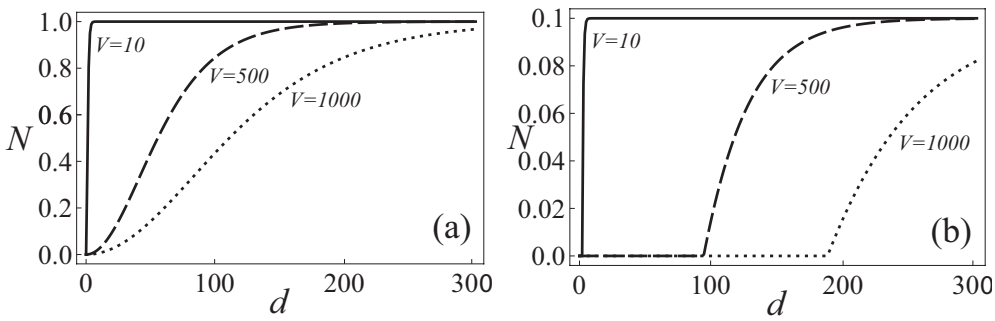

Fig. 4: The NPT of the locally projected state of $\rho^{TT(+)}$ versus the displacement d with (a) $r = 1$ and (b) $r = 0.1$. The amplitude of the projection basis is $\gamma = 2$ as in Figs. 2 and 3. Each curve corresponds to $V = 10(\text{solid}), 500(\text{dashed}),$ and $1000(\text{dotted})$. Nonzero value of d much larger than $\sqrt{V}$ is required to observe entanglement compared to $\rho^{BS(+)}$ cases.

the basis $(|0\rangle \pm |1\rangle)/\sqrt{2}$. The resultant state is

$$\begin{aligned}
&\rho^{TT(\pm)} = \\
&N\big\{\rho_a^{th}(V,d)\otimes\rho_b^{th}(V,d) + \rho_a^{th}(V,-d)\otimes\rho_b^{th}(V,-d) \\
&\pm r\sigma_a(V,d)\otimes\sigma_b(V,d) \pm r\sigma_a(V,-d)\otimes\sigma_b(V,-d)\big\},
\end{aligned} \tag{3.21}$$

We also project this state into a subspace spanned by sets $\{|+\rangle_\gamma, |-\rangle_\gamma\}$ for each mode, then calculate the NPT which is presented in Fig. 4. Again, an initial microscopic state with any value of $r > 0$ is useful to generate entanglement between thermal states regardless of V. Here, however, a condition of $d \gg \sqrt{V}$ is required to clearly observe entanglement.

3.3.2 Entangling two thermal states

We now come to a natural question: Can two highly mixed states, when their purities become arbitrarily small, still be entangled through a direct unitary interaction? We here simply prepare two thermal states in each mode then act cross-Kerr interaction directly. This type of state is considered for observing nonlocality of multipartite entangled thermal states [58]. In order to calculate the effect of the interaction, we first point out that two-mode states where each mode has a definite photon number parity are eigenstates of the cross-Kerr interaction for time $t = \pi/\chi$ so that

$$U_{\text{Kerr}} = e^{i\pi\hat{a}^\dagger\hat{a}\hat{b}^\dagger\hat{b}} = (-1)^{\hat{a}^\dagger\hat{a}\hat{b}^\dagger\hat{b}}. \tag{3.22}$$

It works as a controlled-phase gate on the $|\pm\rangle_\gamma$ basis where $|\pm\rangle_\gamma$ is defined in the above Eq. (3.18) [59]: $U_{\text{Kerr}}\,|+\rangle_\gamma\,|\pm\rangle_\gamma = |+\rangle_\gamma\,|\pm\rangle_\gamma$ and $U_{\text{Kerr}}\,|-\rangle_\gamma\,|\pm\rangle_\gamma = \pm\,|-\rangle_\gamma\,|\pm\rangle_\gamma$. Based on this, we calculate the evolution of the two thermal sates under U_{Kerr} as

$$U_{\text{Kerr}}|\alpha\rangle|\beta\rangle = \frac{1}{2}\big(|\alpha\rangle|\beta\rangle + |\alpha\rangle|-\beta\rangle + |-\alpha\rangle|\beta\rangle - |-\alpha\rangle|-\beta\rangle\big) \equiv |\psi\rangle \tag{3.23}$$

and then the total state after the interaction is

$$\rho^\psi = \int d^2\alpha d^2\beta P_\alpha^{th}(V,d) P_\beta^{th}(V,d) |\psi\rangle\langle\psi|. \tag{3.24}$$

The locally projected density matrix with basis $\{|+\rangle_\gamma, |-\rangle_\gamma\}$ is

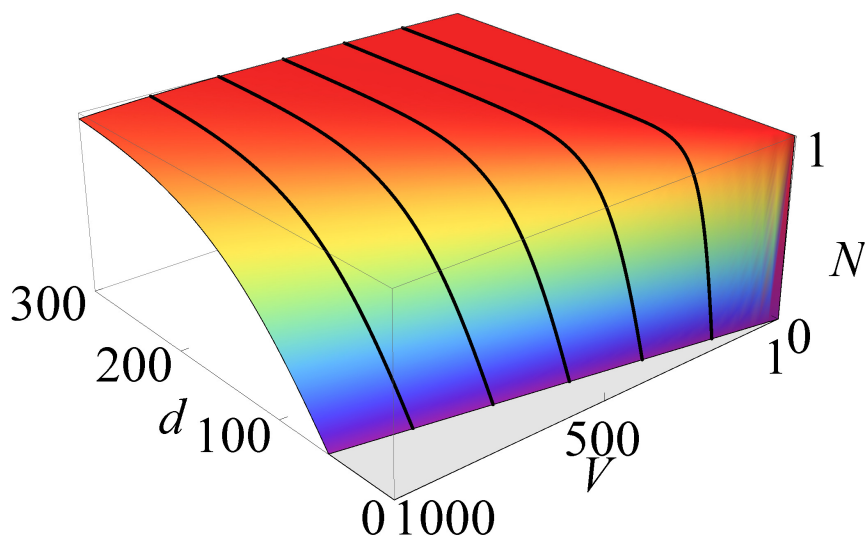

Fig. 5: The NPT of ρ_γ^ψ with $\gamma = 2$. In this case V is the only parameter that adjusts the purities of both parties simultaneously. We can always obtain the entanglement even in $V \to \infty$ limit with sufficient displacement $d \gg \sqrt{V}$. This indicates that nonzero purity of the system is sufficient to generate entanglement.

$$\rho_{\gamma}^{\psi} = \begin{pmatrix} X_{\gamma}^2 & X_{\gamma}S_{\gamma} & S_{\gamma}X_{\gamma} & -S_{\gamma}^2 \\ X_{\gamma}S_{\gamma} & X_{\gamma}Y_{\gamma} & S_{\gamma}^2 & -S_{\gamma}Y_{\gamma} \\ S_{\gamma}X_{\gamma} & S_{\gamma}^2 & Y_{\gamma}X_{\gamma} & -Y_{\gamma}S_{\gamma} \\ -S_{\gamma}^2 & -S_{\gamma}Y_{\gamma} & -Y_{\gamma}S_{\gamma} & Y_{\gamma}^2 \end{pmatrix} \tag{3.25}$$

where $X_{\gamma} = C_{\gamma} + R_{\gamma}$ and $Y_{\gamma} = C_{\gamma} - R_{\gamma}$ in terms of C_{γ}, S_{γ}, and R_{γ} defined in Eq. (3.18).

We plot the results in Fig. 5, which shows that entanglement is generated even in the high temperature limit as far as $d \gg \sqrt{V}$. We observe that two thermal states at arbitrarily high temperatures are entangled through a direct unitary interaction as far as the condition, $d \gg \sqrt{V}$, is satisfied.

3.4 Macroscopic quantumness of entangled thermal states

In preceding sections, we have verified that entanglement is generated between a microscopic state and a thermal state, or even in two identical thermal states with an arbitrarily high temperature. However, the entanglement verification method we employ (acting local projections on infinite dimensional systems) was a sufficient, but not a necessary condition for the presence of entanglement in a give quantum state. That is because a local projection never increases the degree of entanglement but can lower the initial amount of entanglement [49]. Furthermore, the concept of entanglement is

not completely equivalent to that of macroscopic quantumness. It means that there might be a set of entangled quantum states, but not necessarily macroscopically quantum or vice versa. Recently, a true measure of macroscopic quantumness for optical systems is devised based on counting oscillations of a given quantum state in its phase space [30]. We will explain details of the measure in Chap. 5 but let us briefly see the explicit form of it. For two mode optical systems, macroscopic quantumness $\mathcal{I}(\rho)$ of a given quantum state ρ is calculated as

$$\mathcal{I}(\rho) = \sum_{i=1}^{2} \text{Tr}[\rho^2 \hat{a}_i^\dagger \hat{a}_i] - \text{Tr}[\rho \hat{a}_i \rho \hat{a}_i^\dagger], \tag{3.26}$$

where $\hat{a}_i$ and $\hat{a}_i^\dagger$ are the annihilation and the creation operator for the i-th mode, each respectively. We apply this measure to ρ^ψ (Eq. (3.24)) and compare the tendency between the entanglement and the macroscopic quantumness. ρ^ψ can be rewritten as

$$\rho^\psi = U_{\text{Kerr}}(\rho^{th} \otimes \rho^{th}) U_{\text{Kerr}}^\dagger \tag{3.27}$$

Since the two modes are mutually symmetric we can simply double the measure for a single mode to obtain that of the total state as

$$\begin{aligned}
\mathcal{I}(\rho^\psi) =& 2\left(\text{Tr}[\rho^{\psi 2} \hat{a}_1^\dagger \hat{a}_1] - \text{Tr}[\rho^\psi \hat{a}_1 \rho^\psi \hat{a}_1^\dagger]\right) \\
=& 2\Big(\text{Tr}[(\rho^{th})^2 \otimes (\rho^{th})^2 U_{\text{Kerr}}^\dagger \hat{a}_1^\dagger \hat{a}_1 U_{\text{Kerr}}] \\
& - \text{Tr}[\rho^{th} \otimes \rho^{th} U_{\text{Kerr}}^\dagger \hat{a}_1 U_{\text{Kerr}} \rho^{th} \otimes \rho^{th} U_{\text{Kerr}}^\dagger \hat{a}_1 U_{\text{Kerr}}]\Big).
\end{aligned} \tag{3.28}$$

By using the identities

$$U_{\text{Kerr}}^{\dagger}\hat{a}_1 U_{\text{Kerr}} = \hat{a}_1 e^{-i\pi\hat{a}_2^{\dagger}\hat{a}_2}$$
$$U_{\text{Kerr}}^{\dagger}\hat{a}_1^{\dagger}\hat{a}_1 U_{\text{Kerr}} = \hat{a}_1^{\dagger}\hat{a}_1, \tag{3.29}$$

we obtain

$$\begin{aligned}\mathcal{I}(\rho^{\psi}) &= 2\Big(\text{Tr}[(\rho^{th})^2\hat{a}_1^{\dagger}\hat{a}_1]\text{Tr}[(\rho^{th})^2] - \text{Tr}[\rho^{th}\hat{a}_1^{\dagger}\rho^{th}\hat{a}_1]\text{Tr}[\rho^{th}e^{i\pi\hat{a}_2^{\dagger}\hat{a}_2}\rho^{th}e^{-i\pi\hat{a}_2^{\dagger}\hat{a}_2}]\Big) \\ &= 2\Big(\text{Tr}[(\rho^{th})^2\hat{a}_1^{\dagger}\hat{a}_1]\mathcal{P}^{th} - \text{Tr}[\rho^{th}\hat{a}_1^{\dagger}\rho^{th}\hat{a}_1]\mathcal{R}^{th}\Big),\end{aligned} \tag{3.30}$$

where $\mathcal{P}^{th} = \text{Tr}[(\rho^{th})^2] = V^{-1}$ is the purity of the thermal state and $\mathcal{R}^{th} = \text{Tr}[\rho^{th}e^{i\pi\hat{a}_2^{\dagger}\hat{a}_2}\rho^{th}e^{-i\pi\hat{a}_2^{\dagger}\hat{a}_2}] = V^{-1}\exp[-4d^2/V]$ is an overlap of oppositely displaced thermal states. All the trace operations can be done by integrations and finally the measure reads

$$\mathcal{I}(\rho^{\psi}) = \frac{1 + V(4d^2 + V - 2) + e^{-\frac{4d^2}{V}}(1 - 4d^2V - V^2)}{4V^3}, \tag{3.31}$$

and its numerical values are depicted in Fig. 6. For $V = 1$, it is identical to an entangled coherent state and $\mathcal{I} = d^2(1 - \exp[-4d^2])$. If the displacement is large so that the overlap between the two coherent state is negligible, the measure becomes proportional to the average photon number $\mathcal{I} \approx d^2 = \langle\hat{n}\rangle$. For an arbitrary temperature (or V) and a large displacement $d \gg 1$, the

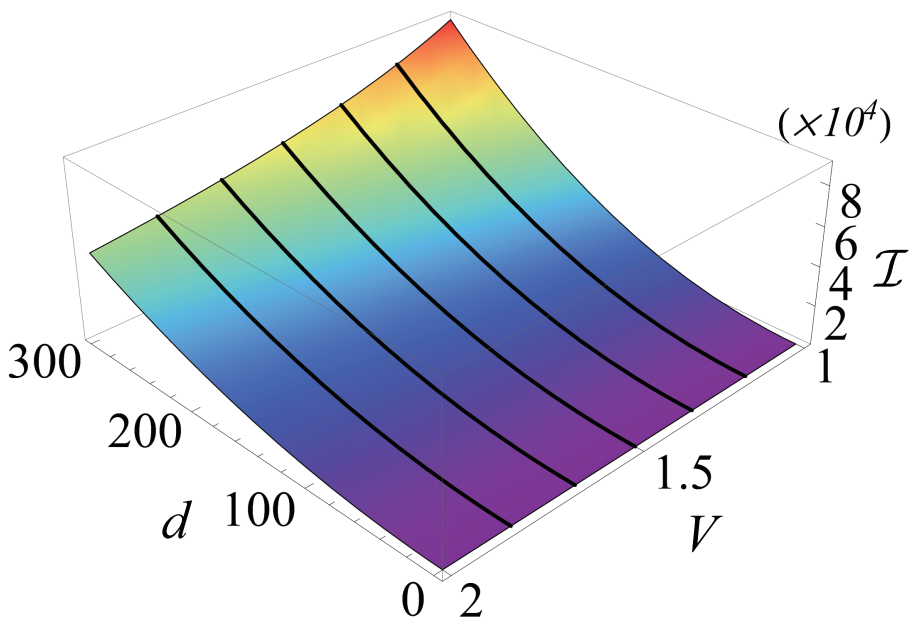

Fig. 6: The macroscopic quantumness $\mathcal{I}$ of ρ^{ψ}. As the temperature like parameter V increases the macroscopic quantumness is lowered. However, we can always remarkable amount of macroscopic quantumness for a large displacement on the initial state.

macroscopic quantumness is simplified as

$$\mathcal{I} \approx (d/V)^2, \tag{3.32}$$

which is very intuitive; the thermal state entanglement is macroscopically quantum for large displacements and low temperatures. In contrast to the entanglement, where we cannot verify the presence of it for the region $d < \sqrt{V}$ as in Fig. 5, we always observe non–vanishing degree of macroscopic quantumness for arbitrary d and V.

3.5 Remarks

In this chapter, we have investigated possibilities of generating entanglement from thermal states with a high temperature. Since a high temperature thermal state has no coherence between photon number states and such photon numbers are large enough to be detected by human eyes, it is regarded a macroscopic classical state [49]. Typically, generating entanglement from such highly classical states is difficult [48, 49, 50, 51, 52, 53]. However, researchers suggested several ideas based on atom–light interaction [49], mechanical mirror and light interaction [51], and utilization of ancillary microscopic states [52, 53]. Among such researches, people thought the purity of the initial state is an critical factor of generation of entanglement even from highly classical state. We further generalized the conditions of initial state so that they can have an arbitrarily low purity for its minimum value. For

atom–light interaction cases, we could not conclude the necessity of the purity since the verification method we used is only a necessary condition. In other words, we cannot be sure that entanglement is not generated when our method is failed to detect them. We moved to purely light–light interactions and found entanglement is generated from displaced high–temperature thermal states if we employ ancillary microscopic superposition. However, such intervention of ancillary state makes the role of the purity unclear. Thus we finally considered the direct interaction between two identical displaced thermal states. We found that entanglement is always generated regardless of the temperature (or purity) of thermal states, once the displacement (which does not modify the initial purity) is enough and the interaction between them is clear. This indicates that we can obtain the same result for an arbitrarily large (up to infinity) temperature, where the purity goes to zero. We also verified it by another measure called macroscopic quantumness [30], which showed a strong evidence compared to the traditional entanglement measure. Therefore, we concluded that the purity of the initial states is not a necessary prerequisite for generating entanglement. It rather critically depends on the interaction type between them.

Chapter 4

Generating Hybrid Entanglement via Photon Addition Scheme

4.1 Concept of hybrid entanglement

The light has two thoroughly different nature of its own. It sometimes behaves like a classical wave, but other times like quantum particles. The most obvious particle like state is the vacuum $|0\rangle$ and the single photon state $|1\rangle$, which represents the absence and presence of the light quantum. Meanwhile, the most classical wave like state is a coherent state $|\alpha\rangle$. It has a completely positive quasi–probability distribution and its expectation value of the quadrature operators follow the classical motions [60, 61]. Since the two different aspects are resemble the quantum mechanical atom and the classical cat in Schrödinger's cat paradox [2], the hybrid entanglement of the form

$$|\Psi(\alpha)\rangle = \frac{1}{\sqrt{2}} \left(|0\rangle |\alpha\rangle + |1\rangle |-\alpha\rangle\right) \tag{4.1}$$

is regarded the closest optical implementation of Schrödinger's cat. However, since the term 'hybrid' generally means any combinations of quantum and classical states, there are various kinds of other hybrid entanglement than we

regard here, and detailed classification and characterizations of them are dealt in Ref. [62]. Note that the state Eq. (4.1) is completely separable for $\alpha = 0$, and is near–maximally entangled for $\alpha \gg 1$ since the overlap between two coherent state part becomes negligible $\langle \alpha | -\alpha \rangle \approx 0$. The more quantitative discussions on the degree of entanglement and macroscopic quantumness is dealt in the later sections of this chapter.

The hybrid entanglement is known to be a very useful resource for quantum information processing [63, 64, 65, 66, 67]. It is utilized for near–deterministic quantum teleportation and universal gate operations for linear optic quantum computing [68] For testing a fundamental aspect of quantum physics as well, it has an advantage [69, 70, 71, 72] for a loophole–free Bell inequality test with inefficient detectors [73, 74]. The most typical way of generating the hybrid entanglement is acting a clean cross–Kerr interaction between a single photon and a coherent state [75, 76, 77]. However, clean and strong cross-Kerr interaction is practically difficult due to the effects of photon losses and phase fluctuations during the interaction [56, 80, 81]. In this chapter, we introduce an alternative way of generating hybrid entanglement using so–called photon addition scheme.

4.2 Amplifying coherent state by photon addition

The most simple and obvious way of amplifying a coherent state is acting a displacement operation, so that an initial coherent state $|\alpha\rangle$ becomes a large

one as $D(\gamma)\,|\alpha\rangle \propto |\alpha+\gamma\rangle$. If we can perform a superposition of two different displacement operations $D(\gamma)+D(-\gamma)$, which is indeed not unitary, we can generate a macroscopic superposition $|\gamma\rangle + |-\gamma\rangle$ by acting it on a vacuum state. However a displacement operation is performed deterministically and there is no way to probabilistically trigger one of those two. In this section, we introduce a method for approximate amplification of coherent states using so-called photon addition scheme.

4.2.1 Photon addition scheme

Photon addition technique is a recently developed scheme that is capable of adding more than one photon into an arbitrary initial state. It utilizes spontaneous parametric downconversion (SPDC) [82] to generate a twin beam, where two light mode called 'signal' and 'idler' always have the same number of photons. As illustrated in Fig. 7, when we detect a single photon from the idler mode, then we can herald that the signal mode contains a single photon as well. If we initially matched the spatial modes of the input and the signal modes, this effectively adds the single photon into the input mode. In mathematical terms, the operation of it is described by acting a creation operator to the input state, $\hat{a}^\dagger\,|\psi\rangle$. Since it is operated in a heralded manner, we can always locate when and where it happened for a series of the same modules. Besides adding a single photon, we can easily subtract a single photon from a quantum state using a beam splitter with a high transmissivity [83, 84]. If we mix the input state $|\psi\rangle$ with the vacuum, then detect a single

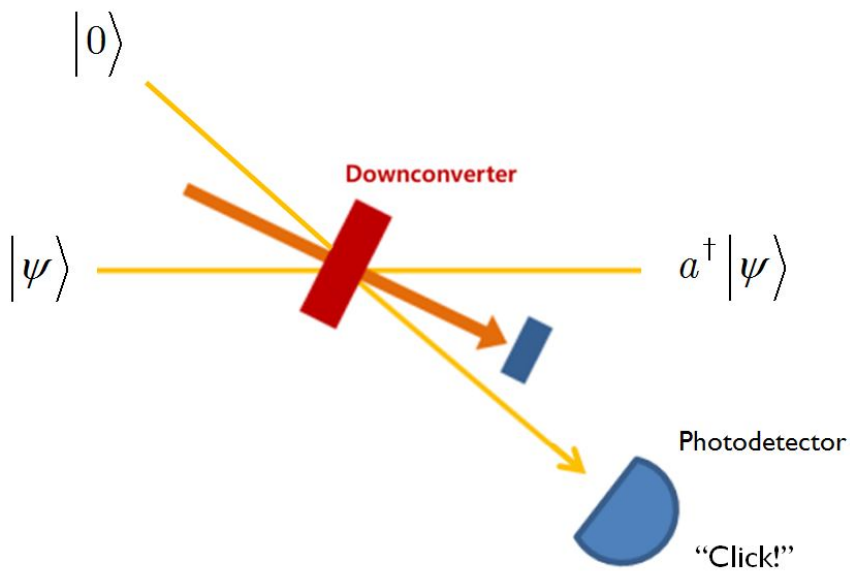

Fig. 7: Schematics of a photon addition module. Nonlinear medium at the center is pumped by a strong laser to generate a twin beam consists of signal and idler modes having the same photon number. If a photodetector detects a single photon from a idler mode, then it is heralded that a single photon is added to the input state $|\psi\rangle$.

photon at the idler output mode of the beam splitter, the remaining state can be approximated as $\hat{a}\,|\psi\rangle$.

This type of conditional single–photon addition and subtraction are used for fundamental proofs of quantum mechanics including quantum to classical transition of optical state [82], quantum cloning of single photons [85], proving bosonic commutation relation ($[\hat{a}, \hat{a}^\dagger] = 1$) for optical states [83, 84]

4.2.2 Coherent state amplification

Suppose we initially have a coherent state with an amplitude α. We can first naively expect that additions of extra photons into the initial coherent state would amplify the amplitude in a sense that the average photon number becomes larger, roughly, as much as the number of photons we added. We investigate such tendency in a more rigorous way. Suppose a n–photon added coherent state

$$|\psi_n\rangle = \frac{1}{\sqrt{\mathcal{N}_n(\alpha)}} a^{\dagger n}\,|\alpha\rangle\,. \tag{4.2}$$

The normalization factor is given as

$$\mathcal{N}_n(\alpha) = e^{-x}\frac{d^n}{dx^n}\left(x^n e^x\right)\Big|_{x=|\alpha|^2} = n! L_n(-|\alpha|^2) \tag{4.3}$$

where L_n is Laguerre polynomial of nth order. Note that the normalization is required since the creation operator $\hat{a}^\dagger$ is not unitary so that modifies the norm of the state vector.

We now search for another coherent state with an amplitude β, that is closest to the photon added coherent state Eq. (4.2) in terms of fidelity. The fidelity between the coherent state $|\beta\rangle$ and n–photon added coherent state $|\psi_n\rangle$ is

$$\begin{aligned}\mathcal{F}_n(\alpha,\beta) &= \mathcal{N}_n^{-1}(\alpha)\left|\langle\beta|\, a^{\dagger n}\,|\alpha\rangle\right|^2 \\ &= \mathcal{N}_n^{-1}(\alpha)\,|\beta|^{2n}\, e^{-(|\alpha|^2+|\beta|^2-\alpha\beta^*-\alpha^*\beta)}. \end{aligned} \tag{4.4}$$

Then we find an extremum that maximize the $\mathcal{F}$ under the fixed α by differentiation,

$$\partial_{\beta^*}\mathcal{F} = (\partial_\beta \mathcal{F})^* = \mathcal{N}_n^{-1}(\alpha)\,|\beta|^{2(n-1)}\left[n\beta + |\beta|^2(\alpha-\beta)\right] = 0. \tag{4.5}$$

Since the first two factors are always positive, the last factor should vanish, $n\beta + |\beta|^2(\alpha-\beta) = 0$. By solving real and imaginary parts of this identity separately, we obtain the optimal value of the target amplitude as

$$\begin{aligned}\beta &= g_n(\alpha)\alpha \\ g_n(\alpha) &= \frac{1}{2} + \sqrt{\frac{1}{4} + \frac{n}{|\alpha|^2}}\end{aligned} \tag{4.6}$$

where $g_n(\alpha)$ is an amplification factor. When $n = 0$ (*i.e.* with no photon added), it is trivial that $g_0(\alpha) = 1$ and $\beta = \alpha$, nothing happens. For a nonzero n, as we qualitatively argued above, $g_n(\alpha)$ is an increasing function of n. This

indicates the optimal amplitude β increases and we are effectively implementing amplification. The maximum fidelity for the optimal amplitude is readily obtained as

$$\mathcal{F}_{max} = \mathcal{N}_n^{-1}(\alpha) g_n^{2n}(\alpha) \left|\alpha\right|^{2n} e^{-|\alpha|^2 (g_n(\alpha)-1)^2}. \tag{4.7}$$

For instances,

$$\begin{aligned} n = 0 &: \mathcal{F}_{max} = 1 = g_0 \\ n = 1 &: \mathcal{F}_{max} = \frac{e^{-(g_1-1)^2\alpha^2}(g_1\alpha)^2}{1+\alpha^2} \\ n = 2 &: \mathcal{F}_{max} = \frac{e^{-(g_2-1)^2\alpha^2}(g_2\alpha)^4}{2+4\alpha^2+\alpha^4}. \end{aligned} \tag{4.8}$$

The numerical plots of the amplification gain and the corresponding fidelity is depicted in Fig. 8 and Wigner distributions of photon–added coherent states are visualized in Fig. 9.

In. Fig 8, one may notice that the amplification factor and the resulting fidelity is in a trade–off relation. For a given initial amplitude of coherent state α, we can more amplify it by adding a larger number of photons as we roughly expected at first. However, as a cost of such larger amplification, the fidelity to the ideal coherent state becomes lower. Therefore, we have to identify a proper value of the initial α to obtain a moderate amplification factor and the fidelity. For example, if the initial amplitude is set by $\alpha = 2$, then resulting state is approximately a coherent state with an amplitude $g\alpha = 2.414$ with the

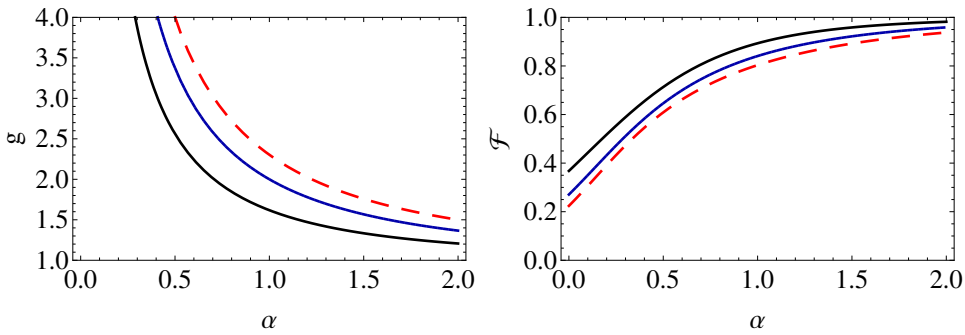

Fig. 8: Plots of the amplification factor $g_n(\alpha)$ and the fidelity $\mathcal{F}$ for the initial amplitude α. When a larger number of photon is added the gain is increased for the same initial amplitude. However, the fidelity is lowered as a trade–off, since adding more photons causes more distortions on the initial shape of a coherent state.

fidelity $\mathcal{F} = 0.98$. If the initial $\alpha = 4$, then $g\alpha = 4.236$ with $\mathcal{F} = 0.998$.

We can see in Fig. 9 the tendency described above in an intuitive manner. Basically, the single photon addition operation makes the original shape in phase space far away from the origin. It resembles throwing a stone at the center of a pond so that objects are shifted from the center due to water wave. However, the original shape is distorted due to irregular propagation of wave so that the Gaussian nature of the initial distribution is lost causing low fidelity.

4.3 Generating hybrid entanglement

Since the photon addition procedure discussed in the previous section is operated in a heralded manner, we can employ multiple identical mod-

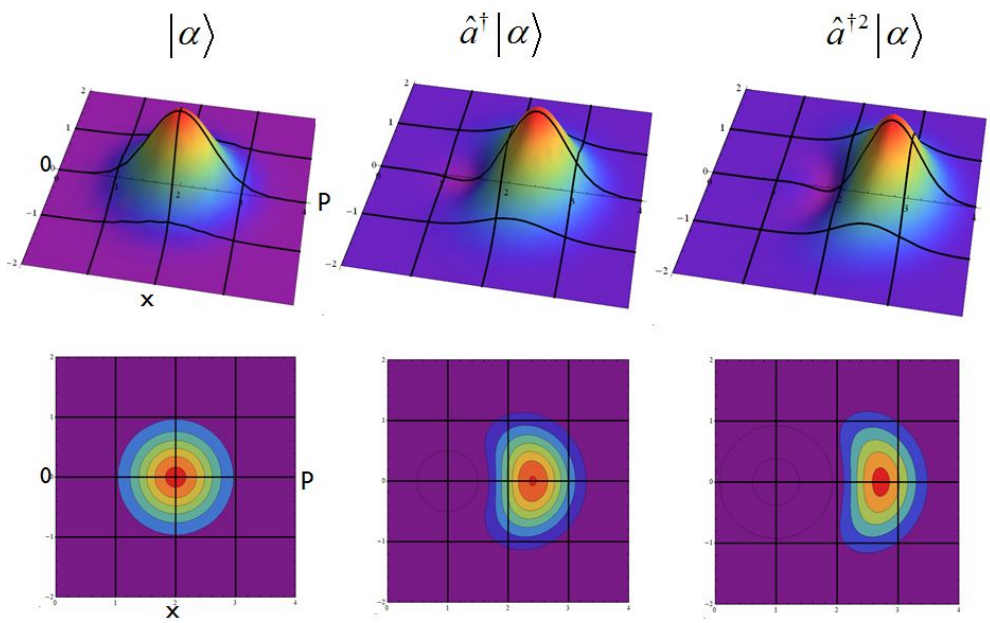

Fig. 9: Wigner distribution of photon–added coherent states. As we successively add single photons, the original distribution of the coherent state is shifted away from the center of the phase space, which indicates that the state is amplified. However, the original Gaussian shape is distorted as a trade–off of acquiring amplification. We can find the optimal amplitude of an ideal coherent state that has the maximum fidelity with the photon–added coherent states as explained in the main text.

ules and utilize combinations of possible triggering events. This idea is the key to approximately generate hybrid entanglement $|0\rangle|\alpha\rangle + |1\rangle|-\alpha\rangle$. Suppose first that we prepare two identical photon-addition modules as in Fig. 10. We input a vacuum $|0\rangle$ and a coherent state $|\alpha_i\rangle$ respectively for each module. If the upper photon–addition module clicks, we can herald the initial vacuum becomes a single photon state $|1\rangle$ while the coherent state remains unchanged. Otherwise, if the lower module clicks, the coherent state obtains an extra single photon and approximately becomes a larger coherent state as discussed in in Sec. 4.2.2. However, if we mix the two heralding signals of the two modules by a beam–splitter with the transmissivity t (and the reflectivity, $r = \sqrt{1-t^2}$), and if only one photon is detected among the two detectors, it is not certain where the photon came out from. Such erasing of path information result the entire output state becomes a superposition of all the possibilities. Thus, the output state is a superposition of $|1\rangle|\alpha_i\rangle$ (where the detected photon is came from the upper module) and $|0\rangle\hat{a}^\dagger|\alpha_i\rangle$ (from the lower module). The coefficient for each possibility is determined by the reflectivity and the transmissivity of the beam–splitter. This is an intuitive consequence since for a very high reflectivity ($r \gg 1$), the detected photon is more likely came from the upper module and reflected toward the upper photo–detector. As a result, the entire output state is (disregarding normalization)

$$r|1\rangle|\alpha_i\rangle + t|0\rangle\hat{a}^\dagger|\alpha_i\rangle\,. \tag{4.9}$$

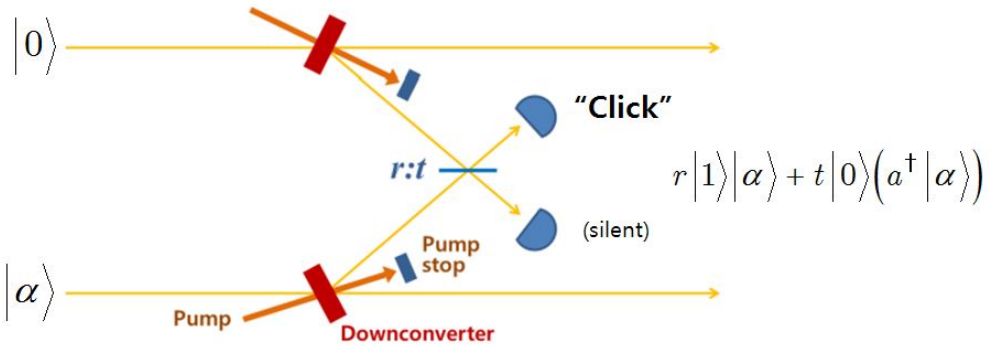

Fig. 10: Scheme for generation of hybrid entanglement using two identical photon-addition modules. The vacuum $|0\rangle$ and a coherent state with amplitude α are given as inputs. If the upper photo–detectors clicks, the entire resultant state becomes $r\,|1\rangle\,|\alpha\rangle + t\,|0\rangle\,\hat{a}^\dagger\,|\alpha\rangle$, disregarding normalization.

If we want to balance the two component states, the transmissivity has to be set as $t = 1/\sqrt{\alpha_i^2 + 2}$ so that the total state is

$$|\Psi_O\rangle = \frac{1}{\sqrt{2}}\left(|1\rangle\,|\alpha_i\rangle + |0\rangle\,\frac{\hat{a}^\dagger\,|\alpha_i\rangle}{\sqrt{\alpha_i^2+1}}\right). \tag{4.10}$$

Notice that the second mode state for the second component $\hat{a}^\dagger\,|\alpha_i\rangle\,/\sqrt{\alpha_i^2+1}$ is identical to Eq. 4.2 with $n = 1$ and is approximately an amplified coherent state $|g\alpha_i\rangle$ with $g = g_1$ given in Eq. (4.6).

Eq. (4.10) is already a form of hybrid entanglement. However, the amplitudes of the coherent state parts are not symmetric with respect to the origin of the phase space. We can symmetrize the state by acting a displacement operation $D_2\,(-(g+1)\alpha_i/2)$ on the second mode so that the state becomes

approximately an ideal hybrid entanglement as

$$|\Psi_S\rangle = D_2\left(-\frac{g+1}{2}\alpha_i\right)|\Psi_O\rangle \approx \frac{1}{\sqrt{2}}\left(|0\rangle\,|\alpha_f\rangle + |1\rangle\,|-\alpha_f\rangle\right), \qquad (4.11)$$

where the final amplitude is given by $\alpha_f = (g-1)\alpha_i$. Note that the displacement operation is local and unitary, thus never changes the degree of entanglement [43, 44, 45] nor the macroscopic quantumness [30] of the asymmetric state.

The fidelity between the symmetrized state and the ideal hybrid entanglement is obtained as

$$\mathcal{F} = |\langle\Psi_S|\Psi(\alpha_f)\rangle|^2 = \frac{1}{4}\left\{1 + \frac{(\alpha+2\alpha_f)^2 e^{-2\alpha_f^2}}{\sqrt{\alpha^2+1}}\right\}^2. \qquad (4.12)$$

Its numerical values are plotted in Fig. 11 for different pairs of the initial and the target amplitudes α_i and α_f. The thick curve on the plot represents the maximal fidelities for a given value of the initial amplitude α_i. Otherwise, those maximal fidelities for a given value of the target amplitude is represented by the dotted line. One might be confused by that there are two different optimal points for a single value of α_i or α_f. For example, the symmetrized model state with the initial amplitude $\alpha_i = 2.0$ has the maximum fidelity $\mathcal{F} \approx 0.991$ to the ideal hybrid entanglement with $\alpha_f = 0.21$. But one may ask what does the point $(\alpha_i, \alpha_f) = (2.0, 0.31)$ on the dotted line indicate. It also can be a valid choice for an experimentalist if he or she wants to obtain

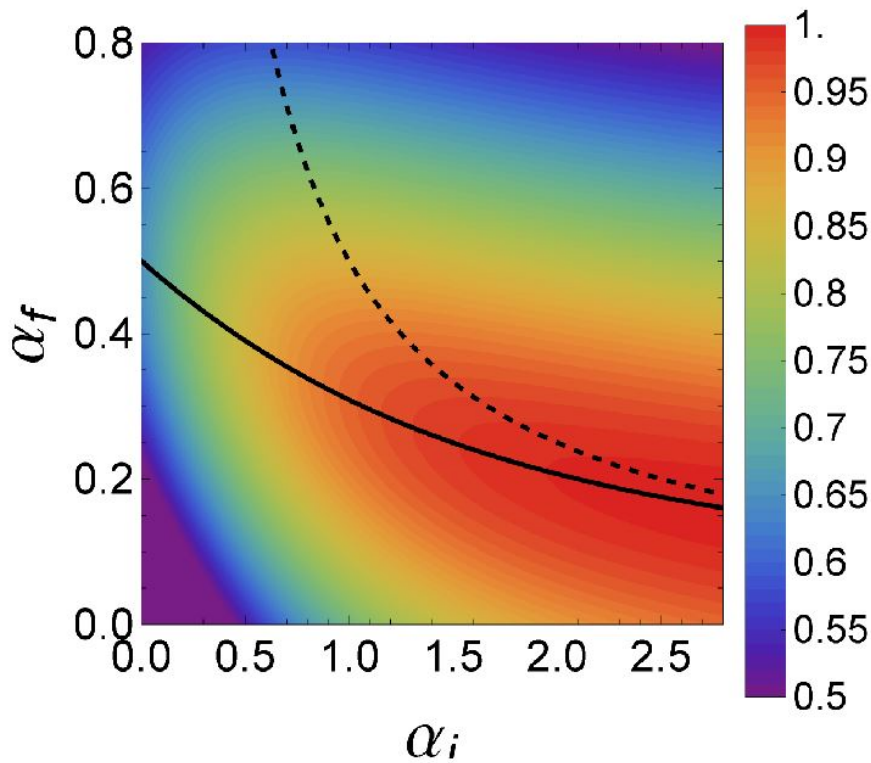

Fig. 11: The fidelity between the symmetrized model state $|\Psi_S\rangle$ and the ideal hybrid entanglement $|\Psi(\alpha_f)\rangle$. The thick line represents the maximal points of the fidelity for a given value of the initial amplitude α_i. In an opposite manner, the dotted line is for a given value of the target amplitude α_f.

a larger amplitude at the price of a lower fidelity.

We calculated the degree of entanglement for the ideal and model states as depicted in Fig. 12. The NPT of the ideal state $|\Psi(\alpha)\rangle$ monotonically increases with respect to α, and becomes saturated to the maximum value 1. Note that for $\alpha = 0$, the NPT is zero because the total state in this case is a product form, $|\Psi(\alpha = 0)\rangle \propto (|0\rangle + |1\rangle) \otimes |0\rangle$. For a large enough value of α, the NPT achieves the maximum as the coherent state parts of the two components become orthogonal $\langle\alpha| - \alpha\rangle \approx 0$ ($\alpha \gg 1$). The red curve in Fig. 12(b) shows the NPT of the model state $|\Psi_S\rangle$ in our scheme against the initial amplitude α_i and the blue curve is for the ideal state that has the maximum fidelity to the model state generated by α_i. Note that for $\alpha_i = 0$, the model state is simply $|\Psi_S(\alpha_i = 0)\rangle = (|0\rangle\,|1\rangle + |1\rangle\,|0\rangle)/\sqrt{2}$, which has the maximum entanglement. However, in this case the fidelity to the ideal state is very low and there is the largest gap between the red and blue curves. In contrast, for a large value of α_i, the gap becomes smaller and eventually the two curves meet. It is because the two components of the superposition $|\alpha_i\rangle$ and $\hat{a}^\dagger\,|\alpha_i\rangle$ become less distinguishable for large α_i bearing less entanglement but high fidelity.

4.4 Macroscopic quantumness of hybrid entanglement

We already discussed a measure of macroscopic quantumness of optical states in Sec. 3.4. Since the quantum states discussed in this chapter is all

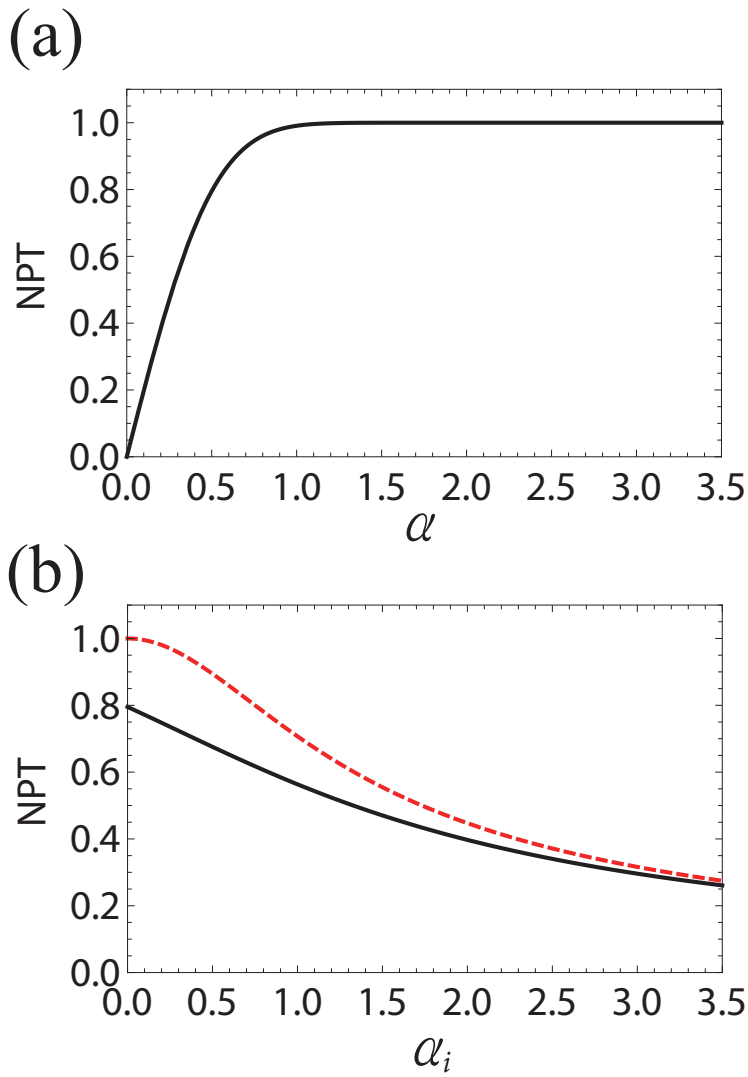

Fig. 12: (a) The negativity of partial transpose (NPT) with respect to the amplitude α of the ideal hybrid state $|\Psi(\alpha)\rangle$ (b) The NPT of the model state $|\Psi_S\rangle$ against the initial amplitude α_i (red–dashed curve). The black curve is the NPT of the ideal hybrid state that has the maximum fidelity to the model state.

pure, the macroscopic quantumness can be calculated as [30]

$$\mathcal{I}(|\psi\rangle) = \sum_{i=1}^{N} \langle\psi|\hat{a}_i^\dagger \hat{a}_i|\psi\rangle - |\langle\psi|\hat{a}_i|\psi\rangle|^2 , \tag{4.13}$$

where N is the number of modes. For the ideal hybrid entanglement $|\Psi(\alpha_f)\rangle$ the macroscopic quantumness reads

$$\mathcal{I}\left(|\Psi(\alpha_f)\rangle\right) = |\alpha_f|^2 + \frac{1}{4}(2 - e^{-4|\alpha_f|^2}). \tag{4.14}$$

Since the final amplitude can be converted to the initial amplitude by the relation $\alpha_f = (g-1)\alpha_i$, we can plot the above equation in terms of α_i. Similarly, the macroscopic quantumness for the model state $|\Psi_S(\alpha_i)\rangle$ is

$$\mathcal{I}\left(|\Psi_S(\alpha_i)\rangle\right) = \frac{1}{4}\left(\frac{|\alpha_i|^2 + 2}{|\alpha_i|^2 + 1}\right)^2 . \tag{4.15}$$

We plotted the macroscopic quatnumness for both cases in Fig. 13. For a special case of $\alpha_i = 0$, the model state is simply $\propto |0\rangle|1\rangle + |1\rangle|0\rangle$. Thus the macroscopic quantumness is the average photon number of the total mode which is 1. Meanwhile, the closest ideal state to this special case of the model state is $|\Psi(\alpha_f = 0.5)\rangle$ of which macroscopic quantumness is less than 1. They both monotonically decrease as the initial amplitude α_i rise and meet together being saturated to the value $1/4$ in analogous to the entanglement case.

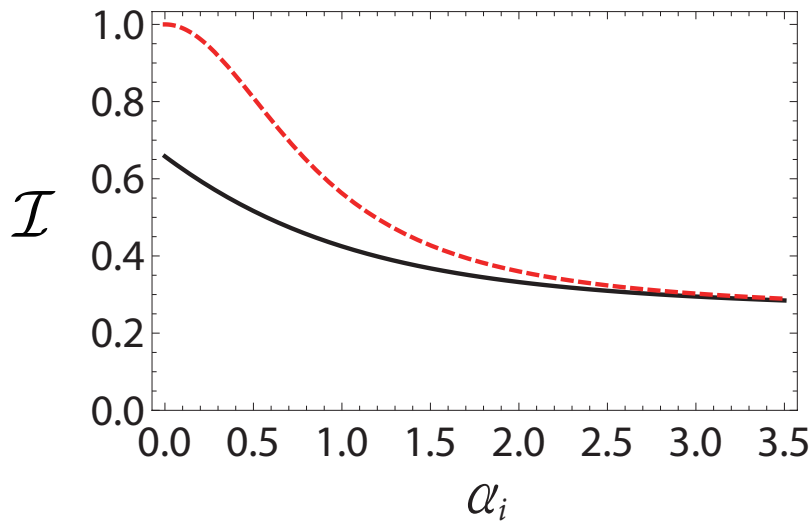

Fig. 13: The macroscopic quantumness $\mathcal{I}$ of the model state $|\Psi_S(\alpha_i)\rangle$ (red–dashed curve), and that of the closest ideal hybrid state $|\Psi(\alpha_f)\rangle$ (black curve). The optimal amplitude of the ideal state is given by $\alpha_f = (g-1)\alpha_i/2$.

4.5 Remarks

Hybrid entanglement is useful not only for demonstrations of fundamental properties of quantum mechanics [69] but also for practical implementations of quantum information processing [68] However, typical generation methods of hybrid entanglement require a highly non–linear interaction called cross–Kerr [75, 76, 77]. Such interaction is practically difficult due to loss of photons and quantum coherence between them [56, 80, 81]. We here suggested a novel way of generating hybrid entanglement via single–photon addition scheme. The single–photon addition scheme utilizes non–linear media to conditionally add an extra photon into an input state that we would like to

manipulate. We found that adding a single photon into an ideal coherent state becomes another approximate coherent state with a larger amplitude, yet the fidelity to an ideal coherent state less than 1. We could select a proper initial amplitude of coherent state, then obtain an amplified amplitude with a large enough fidelity. One important property of single–photon addition module is that we can always herald the event that the extra photon is added to the input state. This enables us to combine two identical modules and mix the signaling beams so that making uncertain where the single photon is added among two input states. Thus the resultant state becomes a superposition of two possibilities that the photon is added into one input state or another. The superposition approximately has the form of hybrid entanglement that we intended to obtain. We can further symmetrize the coherent state part of the entanglement by acting a displacement operation by an preliminarily given amount. Our idea is experimentally realized by optical time–binning method in Ref. [86], and theoretical possibility of further amplification of the coherent part is analyzed in there [86].

Chapter 5

Quantifying Macroscopic Quantumness of Spin States

5.1 Introduction

As illustrated in Schrödinger's famous cat paradox [2], quantum mechanics does not preclude the possibility of a macroscopic object being in a quantum superposition. There has been interesting progress in generating macroscopic superpositions using atomic/molecular systems [3, 4], superconducting circuits [5, 6], and optical setups [7, 10, 11]. On the other hand, how to sharply define and quantify "macroscopic quantumness" or "quantum macroscopicity" is a very slippery issue [88]. There are several proposals for quantification of macroscopic quantum superposition [30, 33, 34, 88, 89, 90, 91, 92, 93, 94, 95, 96, 97, 98, 99, 100, 101] and reviews of them [97, 103]. However, most of them are applicable only for pure states or even more restricted forms of states. Recently, measure for bosonic system is proposed based on interference fringes in phase space [30]. For spin systems, a measure of macroscopic quantumness applicable for arbitrary mixed states is suggested in terms of non–classical parameter estimation represented by

quantum Fisher information (QFI) [33]. However, QFI based measure might detects a biased set of macroscopic quantum states as it is focused on a specific macroscopic quantum phenomenon. We here propose a general measure of macroscopic quantumness from interference fringes in its phase space. We further prove that our measure is directly related to the maximum purity decay rate under Lindblad type of decoherence model. Our measure has less computational complexity compared to QFI based measure since eigen–decomposition of the density matrix is not required. In search of genuine macroscopic quantum phenomena, we investigate macroscopic quantumness of many–body spin states while the system undergoes quantum phase transition (QPT). In contrast to accumulation of microscopic quantum effects such as Debye's T^3 law, superconductivity, or superfluidity [34], QPT turned to be a genuine macroscopic quantum phenomena where the entire effect cannot be explained by a subset of constituting particles.

5.2 Review of macroscopic quantumness for optical states

We first review a measure of macroscopic quantumness based on interference fringes in phase space for an arbitrary mixed state of optical systems. It is devised based on heuristic observations that typical macroscopic quantum superpositions exhibit remarkable interference fringes in phase space illustration. For the most apparent example, consider a macroscopic quantum

superposition consists of two oppositely–phased coherent states $|\pm\alpha\rangle$ as

$$\mathcal{N}(|\alpha\rangle + |-\alpha\rangle), \tag{5.1}$$

where $\mathcal{N} = 1/\sqrt{2 + 2\exp[-|\alpha|^2]}$ is a normalization factor. Since the phase of a large amplitude coherent state is macroscopically observable and distinguishable quantity by a classical interferometer, it can be though as an optical version of Schrödinger's cat state. However, one can also imagine an imperfect superposition of the two coherent state components

$$\mathcal{N}' \left\{|\alpha\rangle\langle\alpha| + |-\alpha\rangle\langle-\alpha| + \Gamma(|\alpha\rangle\langle-\alpha| + |-\alpha\rangle\langle\alpha|)\right\}, \tag{5.2}$$

now the normalization is $\mathcal{N}' = (2 + 2\Gamma\exp[-2|\alpha|^2])^{-1}$. The perfect superposition Eq. (5.1) is a special case of Eq. (5.2) with $\Gamma = 1$.

The difference of coherent and incoherent superposition can be seen visually via Wigner quasi–probability distribution. A quantum state of an optical system represented by a density matrix ρ can be equivalently transformed into Wigner function defined as

$$W(\alpha) = \frac{1}{\pi}\int d^2\xi e^{\xi^*\alpha - \alpha^*\xi}\chi(\xi), \tag{5.3}$$

where $\chi(\xi) = \mathrm{Tr}[\rho\hat{D}(\xi)]$ is a characteristic function associated to a displacement operator $\hat{D}(\xi) = \exp[\xi\hat{a}^\dagger - \xi^*\hat{a}]$. In Fig. 14, we plotted Wigner distributions of Eq. (5.1) for $\alpha = 2, 4$ and Eq. (5.2) for $\alpha = 4$ with $\Gamma = 1/2, 0$. As

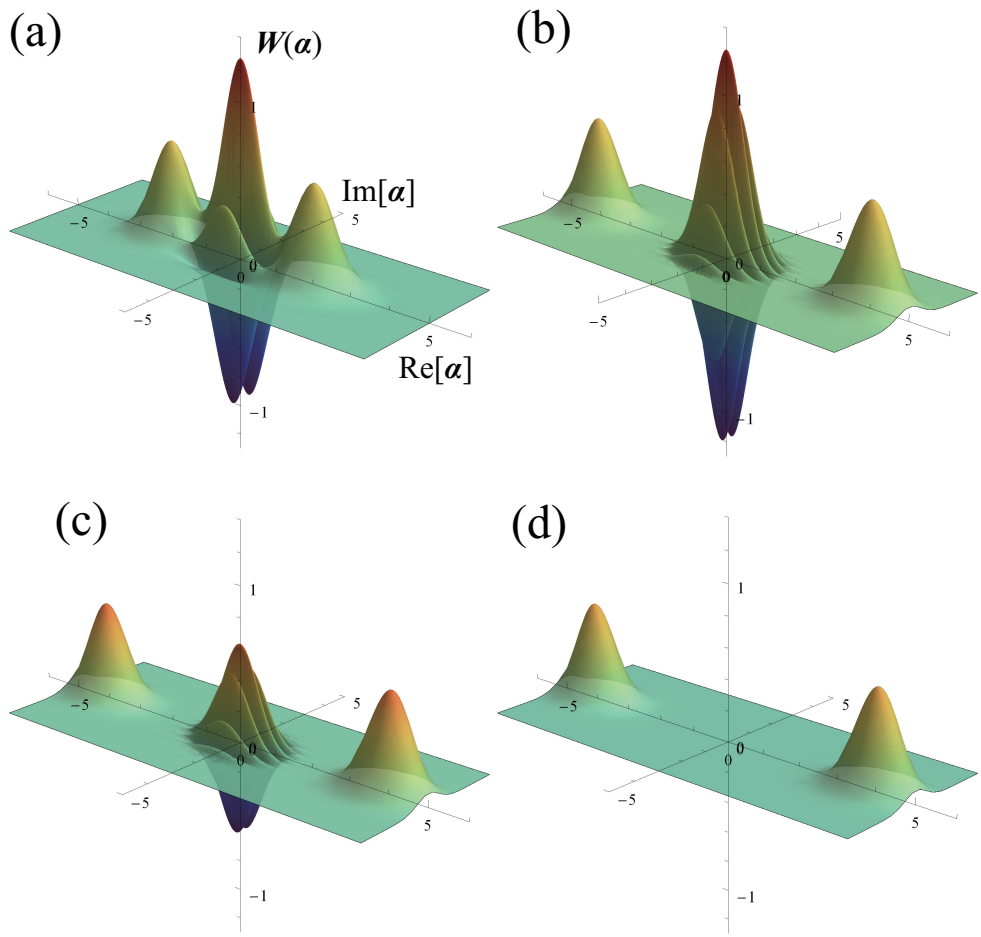

Fig. 14: Wigner functions of $\mathcal{N}(|\alpha\rangle + |-\alpha\rangle)$ with (a) $\alpha = 2$ and (b) $\alpha = 4$. (c) is partially decohered SCS of $\alpha = 4$ with factor $\Gamma = 1/2$ and (d) is fully decohered classical mixture $\frac{1}{2}\{|\alpha\rangle\langle\alpha| + |-\alpha\rangle\langle-\alpha|\}$ of $\alpha = 4$.

the magnitude of α increases the distance between two major peaks becomes larger proportional to $|\alpha|$. At the same time, if the coherence is perfectly maintained, the frequency of interference fringe at the center of phase space also becomes larger so that we can observe remarkable oscillations. In contrast, if the coherence is somewhat lower than the perfect case ($\Gamma < 1$), the interference fringe is damped proportional to Γ, and completely disappears when the state loses the coherence and becomes a statistical mixture ($\Gamma = 0$).

One might notice that Wigner function Eq. (5.3) is a Fourier transform of the characteristic function $\chi(\xi)$. In other words, Wigner function is a linear combination of oscillating basis $\exp[\xi^*\alpha - \alpha^*\xi]$ having the complex frequency ξ weighted by $\chi(\xi)$. Therefore, a large macroscopic quantum superposition showing more frequent interference fringes in the phase space will contain a dominant oscillating basis with a large value of the complex frequency $|\xi|$. Lee and Jeong then defined a measure of macroscopic quantumness for a single mode optical state as following

$$\begin{aligned}\mathcal{I}(\rho) &\propto \int \text{(frequency size)} \times \text{(frequency amplitude)} \\ &\equiv \frac{1}{2\pi}\int d^2\xi\ (|\xi|^2 - 1)|\chi(\xi)|^2. \end{aligned} \tag{5.4}$$

The extension of the measure to an arbitrary N–mode quantum state is

$$\mathcal{I}\left(\rho\right) = \frac{1}{2\pi^N}\int d^2\boldsymbol{\xi} \sum_{i=1}^{N}\left[|\xi_i|^2 - 1\right]|\chi\left(\boldsymbol{\xi}\right)|^2 \tag{5.5}$$

where $\chi(\boldsymbol{\xi}) = \mathrm{Tr}[\rho D_1(\xi_1) D_2(\xi_2) \cdots D_N(\xi_N)]$ with $\boldsymbol{\xi} = (\xi_1, \xi_2, \cdots, \xi_N)$.

It is proven [30] that the measure is directly related to a decoherence process of the system so that the measure is reduced to

$$\mathcal{I}(\rho) = -\mathrm{Tr}\left[\rho \mathcal{L}(\rho)\right], \tag{5.6}$$

where $\mathcal{L}(\rho)$ is the superoperator in the Lindblad form of a vacuum-environment decoherence model [104, 105]:

$$\frac{d\rho}{d\tau} = \mathcal{L}(\rho) = \sum_{m=1}^{M} \left[\hat{a}_m \rho \hat{a}_m^\dagger - \frac{1}{2} \rho \hat{a}_m^\dagger \hat{a}_m - \frac{1}{2} \hat{a}_m^\dagger \hat{a}_m \rho \right], \tag{5.7}$$

where τ = (decay rate)$\times$(time) is the dimensionless time. If we let $\mathcal{P} = \mathrm{Tr}\left[\rho^2\right]$ be the purity of state ρ, $\mathcal{I}(\rho)$ is found to be the decreasing rate of the purity for ρ as

$$\mathcal{I}(\rho) = -\frac{1}{2} \frac{d\mathcal{P}(\rho)}{d\tau}. \tag{5.8}$$

Having known that the measure of macroscopic quantumness can be written in terms of Wigner function and the density matrix equivalently, the most practical way of calculating $\mathcal{I}(\rho)$ is

$$\mathcal{I}(\rho) = \sum_{i=1}^{N} \mathrm{Tr}[\rho^2 \hat{a}_i^\dagger \hat{a}_i] - \mathrm{Tr}[\rho \hat{a}_i \rho \hat{a}_i^\dagger]. \tag{5.9}$$

Furthermore, if the quantum state is pure ($\rho^2 = \rho$), the measure is reduced as

$$\mathcal{I}(\rho) = \sum_{i=1}^{N} \langle \hat{a}_i^\dagger \hat{a}_i \rangle - |\langle \hat{a}_i \rangle|^2 . \tag{5.10}$$

If the total state has a definite purity of the total photon number, then the second term $\langle \hat{a}_i \rangle$ will vanish regardless of the mode index i. Then the measure is simply identical to sum of the average photon number for each mode,

$$\mathcal{I}(\rho) = \sum_{i=1}^{N} \langle \hat{n}_i \rangle. \tag{5.11}$$

This special case indicates that the degree of macroscopic quantumness increases proportional to the system size (*i.e.* the average photon number) once the perfect coherence is guaranteed (*i.e.* the state is pure) and the parity is not ambiguous.

One other possibility that we can understand the measure in an intuitive way is by looking at it in terms of quadrature (position, momentum) operators $\hat{x}$ and $\hat{p}$. Since $\hat{a} = \hat{x} + i\hat{p}$ and $\hat{a}^\dagger = \hat{x} - i\hat{p}$, the compact form of $\mathcal{I}$ Eq. (5.9) can be written as

$$\begin{aligned} \mathcal{I}(\rho) &= \mathrm{Tr}[\rho^2 \hat{x}^2] - \mathrm{Tr}[\rho \hat{x} \rho \hat{x}] + \mathrm{Tr}[\rho^2 \hat{p}^2] - \mathrm{Tr}[\rho \hat{p} \rho \hat{p}] - 1 \\ &= \int dx dx' (x - x')^2 \left| \langle x|\rho|x' \rangle \right|^2 + \int dp dp' (p - p')^2 \left| \langle x|\rho|x' \rangle \right|^2 - 1, \end{aligned} \tag{5.12}$$

where we used the expansion of the operators $\hat{x}$ and $\hat{p}$ into their eigen spectrum $\hat{x} = \int dx x \, |x\rangle\langle x|$ and for $\hat{p}$ as well in the same manner. We already noted that the measure $\mathcal{I}$ captures both the degree of quantum coherenece and the macroscopic size of the quantum state through some examples. In Eq. (5.12), such properties are now mathematically obvious. The first factor $(x-x')^2$ in the first integral represents *'distinctiveness'* of the two component state $|x\rangle$ and $|x'\rangle$. It quantifies how two outcome values are distant. Meanwhile, the second factor in the integral represents *'quantum coherence'* of the two components. Thus the measure $\mathcal{I}$ results a large value if the quantum state ρ exhibit a large coherence of $|\langle x|\rho|x'\rangle|^2 \approx 1$ for very distinct basis $(x-x')^2 \gg 1$. This argument is also applied to the conjugate basis of $\hat{p}$ as it is clear in Eq. (5.12).

5.3 Macroscopic quantumness of spin states

5.3.1 Wigner distribution of spin states

Wigner distribution of bosonic state gives the complete information of probability distribution of any possible measurement on the bosonic mode. Likewise, there is a well–established Winger distribution also called Stratonovich–Weyl distribution. For a given single spin–S particle, Wigner distribution is defined as

$$W(\mathbf{n}) = \sqrt{\frac{4\pi}{2S+1}} \sum_{L=0}^{2S} \sum_{M=-L}^{L} Y_{L,M}(\mathbf{n}) \, \chi^{(S)}_{L,M}. \tag{5.13}$$

Here, $Y_{L,M}(\mathbf{n})$ denotes spherical harmonics parametrized by a three dimensional unit vector $\mathbf{n}$=(sinθcosϕ, sinθsinϕ, cosθ). In similar to the bosonic Wigner distribution, $\chi^{(S)}_{L,M} = \text{Tr}\left[\hat{T}^{(S)\dagger}_{L,M}\rho\right]$ is the characteristic function of a given quantum state ρ. It is generated by the irreducible tensor operators $\hat{T}^{(S)}_{L,M}$ for the SU(2) group of which matrix components are represented as

$$\langle S,m|\,\hat{T}^{(S)}_{L,M}\,|S,m'\rangle = \sqrt{\frac{2L+1}{2S+1}}C^{S,m'}_{S,m;L,M}, \tag{5.14}$$

where $C^{S,m'}_{S,m;L,M}$ being Clebsch-Gordan coefficients. $|S,m\rangle$ is an eigenstate of the z-component spin operator $\hat{S}_z\,|S,m\rangle = m\,|S,m\rangle$ and $\hat{S}^2\,|S,m\rangle = S(S+1)\,|S,m\rangle$. For simplicity we work with a natural unit $\hbar = 1$ throughout the thesis. Note that $W(\mathbf{n})$ is a real function and normalized as

$$\frac{2S+1}{4\pi}\int d\Omega W(\mathbf{n}) = 1, \tag{5.15}$$

where the integration is done over the solid angle $d\Omega = \sin\theta d\theta d\phi$. Since the spherical harmonics satisfy orthogonality relation,

$$\int d\Omega Y_{L,M}Y^*_{L',M'} = \delta_{L,L'}\delta_{M,M'}, \tag{5.16}$$

we can inversely obtain the characteristic function from Wigner function as,

$$\begin{aligned}
&\sqrt{\frac{2S+1}{4\pi}}\int d\Omega Y^{*}_{L,M}(\mathbf{n})W(\mathbf{n}) \\
&= \sum_{L',M'}\int d\Omega Y_{L',M'}(\mathbf{n})Y^{*}_{L,M}(\mathbf{n})\chi^{(S)}_{L',M'} \\
&= \sum_{L',M'}\delta_{L,L'}\delta_{M,M'}\chi^{(S)}_{L',M'} \\
&= \chi^{(S)}_{L,M}.
\end{aligned} \tag{5.17}$$

Furthermore, the original density matrix can be obtained via the inversion formula:

$$\rho = \sqrt{\frac{2S+1}{4\pi}}\sum_{L=0}^{2S}\sum_{M=-L}^{L}\hat{T}^{(S)}_{L,M}\int d\Omega Y^{*}_{L,M}(\mathbf{n})W(\mathbf{n}). \tag{5.18}$$

For a given Wigner distribution, we can calculate the expectation values of any measurement operator $\hat{f}$ as

$$\langle\hat{f}\rangle = \text{Tr}\left[\hat{f}\rho\right] = \frac{2S+1}{4\pi}\int d\Omega W_{f}(\mathbf{n})W(\mathbf{n}), \tag{5.19}$$

through so–called Wigner symbol of the operator $\hat{f}$, $W_{f}(\mathbf{n})$, which is defined as same as Eq. (5.13) except that the characteristic function is given as $\chi^{(S)}_{L,M} = \text{Tr}\left[\hat{T}^{(S)\dagger}_{L,M}\hat{f}\right]$.

5.3.2 Measure of macroscopic quantumness of spin states

We see that the essential elements to quantify macroscopic quantumness for bosonic system is frequency amplitude and magnitude contained in phase space of a given quantum state. In order to extract such key factors from spin Wigner distribution as well, we need to analyze similarity between mathematical structures of the two different Wigner distributions in the finite and the infinite dimensional systems. One can notice that in Winger function of spin states Eq. (5.13), integration over infinite domain spanned by a complex argument ξ is replaced by discrete summation over L and M. This is because the number of basis $\exp[\xi^*\alpha - \alpha^*\xi]$ for the bosonic system is infinite, whereas the number of basis for spin–S particle is $(2S+1)^2$. For the harmonic oscillatory basis $\exp[\xi^*\alpha - \alpha^*\xi]$, it is clear that the real and imaginary components ξ_r and ξ_i of ξ is the frequency of oscillations. However, the concept of *frequency* is not that obvious for the spherical harmonics as it is a complex combination of trigonometric functions where a clear periodicity is not guaranteed. In order to identify the frequency from the spin Wigner function, it is definitely helpful to visualize of them for several spin states. Obviously, the most macroscopic superposition of a single spin–S particle is

$$\frac{1}{\sqrt{2}}\left(|S,S\rangle + |S,-S\rangle\right), \tag{5.20}$$

which is superposition of the maximum and minimum possible outcome of z–axis spin measurement. For a large enough value of S, the two components

$|S, \pm S\rangle$ are distinguishable as like two opposite directions of a magnet; which are *macroscopically distinguishable* states. If Eq. (5.20) undergoes dephasing decoherence, the quantum coherence between the two component states (*i.e.* diagonal elements of the density matrix) will decay for time as

$$\rho = \frac{1}{2}\left[|S,S\rangle\langle S,S| + |S,-S\rangle\langle S,-S| + \gamma\left(|S,S\rangle\langle S,-S| + |S,-S\rangle\langle S,S|\right)\right], \tag{5.21}$$

where $\gamma \in [0,1]$ is a decaying factor, which is 1 for the perfect superposition and 0 for the complete classical mixture.

We now visualize Wigner distributions of Eq. (5.20) and Eq. (5.21) for some chosen value of S as depicted in Fig. 15. One can observe that there are balloon–shaped two major peaks heading $\pm z$ directions which represent quasi–probabilities of the two main components $|S, \pm S\rangle$. In addition, there are many small shapes lying on xy–plane resemble petals of flowers. These are products of coherent interference of the two main components. As the state loses quantum coherence due to dephasing decoherence, the magnitude of diagonal elements are decreased and the size of the petals as well. The petals totally disappear when the state loses coherence and becomes a complete classical mixture ($\gamma = 0$). These serial observations are evidence that interference fringes in phase space are obviously indications of quantum coherence. One might notice that the many–fold rotational symmetry of the interference patterns comes from ϕ-periodicity of spherical harmonics $Y_{L,M}(\mathbf{n})$ of Wigner distribution. An explicit term that contains ϕ only ap-

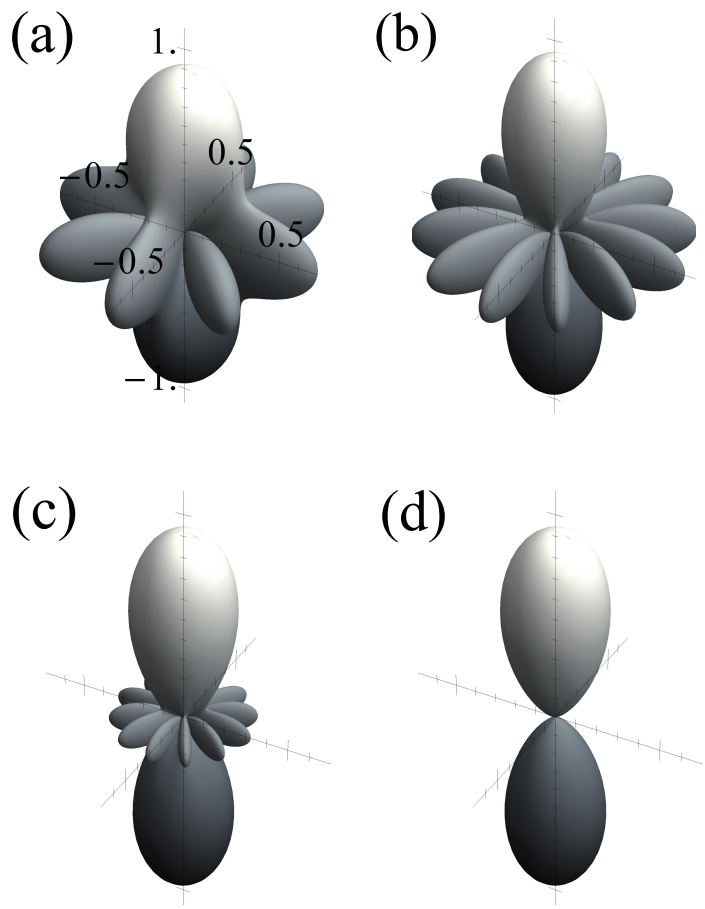

Fig. 15: Wigner distribution of $(|S,S\rangle + |S,-S\rangle)/\sqrt{2}$ for (a) $S = 2$ and (b) $S = 3$. The distribution consists of two peaks in $\pm z$ directions and interference fringes around z–axis. When the state of the panel (b) becomes $\{|3,3\rangle\langle 3,3| + |3,-3\rangle\langle 3,-3| + \gamma(|3,3\rangle\langle 3,-3| + |3,-3\rangle\langle 3,3|)\}$ due to dephasing decoherence, the interference fringe becomes smaller as in the panel (c) with $\gamma = 1/2$. A fully decohered complete mixture has no interference fringe as in the panel (d).

pears as $\exp[\pm iM\phi]$. Therefore, we take M^2 as frequency magnitude for a macroscopic quantumness of spin states. Accordingly, the characteristic function that weights the spherical harmonics, the unclear oscillation basis, can be utilized as a weight of the frequency. We take the weight of the frequency proportional to $\left|\chi^{(S)}_{L,M}\right|^2$. Thus, normalized weight should be

$$\frac{\left|\chi^{(S)}_{L,M}\right|^2}{\sum_{L'=0}^{2S}\sum_{M'=-L'}^{L'}\left|\chi^{(S)}_{L',M'}\right|^2}. \tag{5.22}$$

We show that the denominator of Eq. (5.22) is identical to purity of the system $\mathcal{P}(\rho) = \text{Tr}[\rho^2]$. By substituting Eq. (5.17) into the denominator of Eq. (5.22) we see that,

$$\begin{aligned}
\sum_{L,M}\left|\chi^{(S)}_{L,M}\right|^2 &= \frac{2S+1}{4\pi}\int d\Omega d\Omega' \left(\sum_{L,M} Y_{L,M}(\mathbf{n})Y^*_{L,M}(\mathbf{n}')\right)W(\mathbf{n})W(\mathbf{n}') \\
&= \frac{2S+1}{4\pi}\int d\Omega d\Omega' \delta(\mathbf{n}-\mathbf{n}')W(\mathbf{n})W(\mathbf{n}') \\
&= \frac{2S+1}{4\pi}\int d\Omega W^2(\mathbf{n}) \\
&= \text{Tr}[\rho^2] = \mathcal{P}(\rho).
\end{aligned} \tag{5.23}$$

We have identified the two essential elements for quantifying macroscopic quantumness for spin states, M^2 for frequency magnitude, and $\mathcal{P}^{-1}\left|\chi^{(S)}_{L,M}\right|^2$ for the amplitude or the weight of it. Therefore, a measure of macroscopic

quantumness would be

$$\begin{aligned}
&\sum \text{(frequency magnitude)} \times \text{(frequency amplitude)} \\
&= \frac{1}{\mathcal{P}} \sum_{L=0}^{2S} \sum_{M=-L}^{L} M^2 \left| \chi_{L,M}^{(S)} \right|^2 .
\end{aligned} \tag{5.24}$$

We can equivalently represent above definition in terms of Wigner distribution instead of the characteristic function by using Eq. (5.17),

$$\begin{aligned}
&\frac{1}{\mathcal{P}} \sum_{L=0}^{2S} \sum_{M=-L}^{L} M^2 \left| \chi_{L,M}^{(S)} \right|^2 \\
&= \frac{1}{\mathcal{P}} \sum_{L=0}^{2S} \sum_{M=-L}^{L} M^2 \chi_{L,M}^{(S)*} \chi_{L,M}^{(S)} \\
&= \frac{1}{\mathcal{P}} \sqrt{\frac{2S+1}{4\pi}} \sum_{L,M} \int d\Omega M^2 Y_{L,M}(\mathbf{n}) W(\mathbf{n}) \chi_{L,M}^{(S)} \\
&= -\frac{1}{\mathcal{P}} \sqrt{\frac{2S+1}{4\pi}} \sum_{L,M} \int d\Omega \frac{\partial^2 Y_{L,M}(\mathbf{n})}{\partial \phi^2} W(\mathbf{n}) \chi_{L,M}^{(S)} \\
&= -\frac{2S+1}{4\pi\mathcal{P}} \sum_{L,M} \int d\Omega Y_{L,M}(\mathbf{n}) \frac{\partial^2 W(\mathbf{n})}{\partial \phi^2} \int d\Omega' Y_{L,M}^*(\mathbf{n}') W(\mathbf{n}') \\
&= -\frac{2S+1}{4\pi\mathcal{P}} \int d\Omega d\Omega' \delta(\mathbf{n}-\mathbf{n}') \frac{\partial^2 W(\mathbf{n})}{\partial \phi^2} W(\mathbf{n}') \\
&= -\frac{2S+1}{4\pi\mathcal{P}} \int d\Omega \frac{\partial^2 W(\mathbf{n})}{\partial \phi^2} W(\mathbf{n}),
\end{aligned} \tag{5.25}$$

where integration by parts is used for the fourth equality. Notice that averaging frequency content by the characteristic function is equivalent to capturing

the *structure* of Wigner function by differential operations; which measure how much the distribution is curvy or oscillating. However, as one can see in the result of Eq. (5.25), it does not extract any dependence of θ of Wigner distribution. It is because we have been focusing on a specific shape of the interference fringe (*i.e.* ϕ–periodicity in Fig. 15) of Wigner distribution, which reveals a clear tendency and a mathematical simplicity. As a result, the *structure capturing* operator appears as $-\partial^2/\partial\phi^2$. Fortunately, we can generalize such a structure capturing operator to include θ–dependence by noticing that $-\partial^2/\partial\phi^2$ is actually z–component angular momentum operator squared $\hat{L}_z^2$ in spherical coordinates, where $\hat{L}_z = -i\partial/\partial\phi$. Thus, we generalized the orientation of this operator as

$$\hat{L}_z^2 \to \hat{L}_{\boldsymbol{\alpha}}^2 = (\alpha_x \hat{L}_x + \alpha_y \hat{L}_y + \alpha_z \hat{L}_z)^2, \tag{5.26}$$

where

$$\begin{aligned} \hat{L}_x &= i \sin\phi \frac{\partial}{\partial\theta} + i \cot\theta \cos\phi \frac{\partial}{\partial\phi} \\ \hat{L}_y &= -i \cos\phi \frac{\partial}{\partial\theta} + i \cot\theta \sin\phi \frac{\partial}{\partial\phi} \end{aligned} \tag{5.27}$$

and $\boldsymbol{\alpha} = (\alpha_x, \alpha_y, \alpha_z)$ is a unit vector with a normalization condition $\|\boldsymbol{\alpha}\|^2 = \alpha_x^2 + \alpha_y^2 + \alpha_z^2 = 1$. A measure should be maximized over all possible directions of $\boldsymbol{\alpha}$ so that it optimally extracts the structure of a given Wigner distribution.

Based on the above arguments, we formally define a measure of macroscopic quantumness for N spin–S states as

$$\mathcal{I}(\rho) \equiv \frac{1}{2NS\mathcal{P}}\Big(\frac{2S+1}{4\pi}\Big)^N \times \max_{\{\boldsymbol{\alpha}^{(i)}\}} \int d\boldsymbol{\Omega}\, W(\{\mathbf{n}_i\})\, \hat{L}^2_{\{\boldsymbol{\alpha}^{(i)}\}} W(\{\mathbf{n}_i\})\,, \tag{5.28}$$

where $d\boldsymbol{\Omega} = d\Omega_1 d\Omega_2 \cdots d\Omega_N$ and $\{\mathbf{n}_i\}$ denotes a set of unit vectors $\{\mathbf{n}_1, \cdots, \mathbf{n}_N\}$ for each particle. The total *structure capturing* operator for many spins is $\hat{L}_{\{\boldsymbol{\alpha}^{(i)}\}} = \sum_i \hat{L}_{\boldsymbol{\alpha}^{(i)}}$, where each local operator is oriented in $\boldsymbol{\alpha}^{(i)}$ direction. The additional factor $(2NS)^{-1}$ is for normalization so that the maximal order of the measure scales with $O(NS)$, which will be justified in later examples. Though our measure is defined in terms of Wigner functions and structure capturing operators represented in terms of angular momentum operators in spherical coordinates, we can prove that the measure can equivalently expressed by the density matrix and spin operators:

$$\begin{aligned}
\mathcal{I}(\rho) &= \frac{1}{NS\mathcal{P}} \min_A \big(\mathrm{Tr}[\rho^2 A^2] - \mathrm{Tr}[\rho A \rho A]\big) \\
&= -\frac{1}{NS\mathcal{P}} \min_A \mathrm{Tr}\left[\rho \mathcal{L}(\rho)\right] \\
&= -\frac{1}{2NS} \min_A \frac{\dot{\mathcal{P}}}{\mathcal{P}}
\end{aligned} \tag{5.29}$$

with a Lindblad type of decoherence channel

$$\frac{d\rho}{d\tau} = \mathcal{L}(\rho) = A\rho A^\dagger - \frac{1}{2}\left(A^\dagger A\rho + \rho A^\dagger A\right) = -[A,[A,\rho]], \tag{5.30}$$

where $A = \sum_{j=1}^{N} A^{(j)}$ with $A^{(j)} = \boldsymbol{\alpha}^{(j)} \cdot \hat{\mathbf{S}}^{(j)}$ being the spin operator of jth site with $\|\boldsymbol{\alpha}^{(j)}\| = 1$. We take τ=(decay rate)$\times$(time) as dimensionless time. Thus the measure Eq. (5.28) has a physical meaning as a percentage decaying rate of the current purity. We prove that for a single spin–S particle Eq. (5.29) is identical to Eq. (5.28) and the extension for the many–particle case is straightforward. For the case of $N = 1$, Eq. (5.29) becomes

$$\begin{aligned}
\mathcal{I}(\rho) &= \frac{1}{S\mathcal{P}} \left(\mathrm{Tr}\left[\rho^2 A^2\right] - \mathrm{Tr}\left[\rho A \rho A\right] \right) \\
&= \frac{1}{S\mathcal{P}} \sum_{i,j=x,y,z} \alpha_i \alpha_j \left(\mathrm{Tr}[\rho^2 S_i S_j] - \mathrm{Tr}[\rho S_i \rho S_j] \right) \\
&= \frac{1}{S\mathcal{P}} \sum_{i,j=x,y,z} \alpha_i \alpha_j \mathrm{Tr}[\rho \hat{f}_{ij}], \qquad (5.31)
\end{aligned}$$

where $\hat{f}_{ij} = ([S_i, S_j\rho] + [\rho S_i, S_j])/2$. Since the trace of any two operators can be calculated as Eq. (5.19), we need to obtain W–symbol of $\hat{f}_{ij}$,

$$\begin{aligned}
W_{f_{ij}} = \mathrm{Tr}[\hat{f}_{ij}\hat{w}(\mathbf{n})] &= \frac{1}{2}\mathrm{Tr}[S_i S_j \rho \hat{w} + \rho S_i S_j \hat{w} - 2 S_j \rho S_i \hat{w}] \\
&= \frac{1}{2}\mathrm{Tr}[\rho \hat{w} S_i S_j + \rho S_i S_j \hat{w} - 2 \rho S_i \hat{w} S_j] \\
&= \frac{1}{2}\mathrm{Tr}[\rho([\hat{w}, S_i] S_j + S_i [S_j, \hat{w}])] \\
&= \frac{1}{2}\hat{L}_i \mathrm{Tr}[\rho \hat{w} S_j] - \frac{1}{2}\hat{L}_j \mathrm{Tr}[\rho S_i \hat{w}], \qquad (5.32)
\end{aligned}$$

where the last equality holds for $[\hat{w}, S_i] = \hat{L}_i \hat{w}$, which is proven in Ref. [107].

When $i = j$, it is further simplified as

$$W_{f_{ii}} = \frac{1}{2}\hat{L}_i \text{Tr}[\rho[\hat{w}, S_i]] = \frac{1}{2}\hat{L}_i^2 \text{Tr}[\rho\hat{w}] = \frac{1}{2}\hat{L}_i^2 W(\mathbf{n}) \tag{5.33}$$

If $i \neq j$, otherwise, we notice that $\hat{f_{ij}}$ always has its symmetric pair $\hat{f}_{ji}$ in Eq. (5.31) so that we can combine them as,

$$\begin{aligned} W_{f_{ij}} + W_{f_{ji}} &= \text{Tr}[(\hat{f_{ij}} + \hat{f}_{ji})\hat{w}] \\ &= \frac{1}{2}\hat{L}_i \text{Tr}\left[\rho[\hat{w}, S_j]\right] + \frac{1}{2}\hat{L}_j \text{Tr}\left[\rho[\hat{w}, S_i]\right] \\ &= \frac{1}{2}\left(\hat{L}_i\hat{L}_j + \hat{L}_j\hat{L}_i\right)\text{Tr}[\rho\hat{w}] \\ &= \frac{1}{2}\left(\hat{L}_i\hat{L}_j + \hat{L}_j\hat{L}_i\right) W(\mathbf{n}) \end{aligned} \tag{5.34}$$

Thus Eq. (5.31) becomes

$$\begin{aligned} \mathcal{I}(\rho) &= \frac{2S+1}{8\pi S\mathcal{P}} \sum_{i,j=x,y,z} \alpha_i\alpha_j \int d\Omega\, W(\mathbf{n})\hat{L}_i\hat{L}_j W(\mathbf{n}) \\ &= \frac{2S+1}{8\pi S\mathcal{P}} \int d\Omega\, W(\mathbf{n})\hat{L}_{\boldsymbol{\alpha}}^2 W(\mathbf{n}) \end{aligned} \tag{5.35}$$

The relation Eq. (5.29) is similar to what the measure for infinite dimensional system showed which was proportional to purity decay rate $d\mathcal{P}/d\tau$ [30], except normalizations. Furthermore, its form is very similar to another exiting measure called q-index [33, 93, 110], where a quantum state is called macroscopic if the trace norm of an operator $[A, [A, \rho]]$ scales with $O(N^2)$ for

an existing A.

If a quantum state is pure (*i.e.* $\rho^2 = \rho$), the measure is further reduced to the variance

$$\mathcal{I} = \max_A \mathcal{V}(A)/(NS) \tag{5.36}$$

, where $\mathcal{V}(A) = \langle A^2 \rangle - \langle A \rangle^2$. It reasonably agrees with our intuition. Commonly, quantum superposition is considered macroscopic if it has large separation between two major peaks of the outcome spectrum, *i.e.* large variations of the outcomes. But employing the variation itself as a measure of macroscopic quantumness does not work even for a basic example. Suppose a pure and a mixed single spin–S states $(|S, S\rangle + |S, -S\rangle)/\sqrt{2}$ and $(|S, S\rangle\langle S, S| + |S, -S\rangle\langle S, -S|)/2$ where the former has a perfect quantum coherence while the latter is a statistical mixture. The variation cannot discriminate the two states since they result the same value S^2. In contrast, our measure gives S for the former and 0 for the latter. We further clarify that the quantum state possessing the maximum macroscopic quantumness is N–party spin–S Greenberger-Horne-Zeilinger (GHZ) state

$$\frac{1}{2}\left(|S, S\rangle^{\otimes N} + |S, -S\rangle^{\otimes N}\right) \tag{5.37}$$

: $\mathcal{I}_{\text{GHZ}} = NS$. Thus a typical spin–$1/2$ GHZ state $|\uparrow\rangle^{\otimes N} + |\downarrow\rangle^{\otimes N}$ is macroscpically quantum as much as a superposition of the far most components of a single spin–$N/2$ particle $|N/2, N/2\rangle + |N/2, -N/2\rangle$ according to our mea-

sure.

5.3.3 Comparison to existing measures

Hereafter, we focus on macroscopic quantumness of multi–qubit states (*i.e.* $S = 1/2$). For simplicity, we normalize $\mathcal{I}_{\text{GHZ}}$ (the maximum value of N spins) to become N rather than $NS = N/2$, which can be done by multiplying 2 to the original definition of $\mathcal{I}(\rho)$.

Recently, another measure of macroscopic quantum state for qubits is suggested based on QFI [33]. If a quantum state possesses large degree of QFI that scales with $O(N^2)$, it can improve the precision of the estimation of unknown parameters beyond the limit that classical physics impose. Therefore, the state is regarded genuinely macroscopically quantum, since it is not classical nor accumulative microscopic quantum. In that sense, quantum Fisher information can be a measure of macroscopic quantumness.

Although our measure and QFI based measure are devised from completely different perspectives, we found very similar mathematical structures of them. Quantum Fisher information is defined as

$$F(\rho, A) = 2 \sum_{i,j=1}^{2^N} (\pi_i - \pi_j)^2/(\pi_i + \pi_j)| \langle i| A |j\rangle |^2, \tag{5.38}$$

where $\pi_i(|i\rangle)$ is i-th eigenvalue(eigenvector) of the density matrix ρ and

$$A = \sum_{j=1}^{N} \boldsymbol{\alpha}^{(j)} \cdot \boldsymbol{\sigma}^{(j)}, \tag{5.39}$$

is a sum of local operators with Pauli operators $\boldsymbol{\sigma}^{(j)}$ for j–th site with $\|\boldsymbol{\alpha}^{(j)} \cdot \boldsymbol{\sigma}^{(j)}\|^2 = \|\boldsymbol{\alpha}^{(j)}\|^2 = 1$. The effective size of macroscopic quantum state is then defined as

$$\mathcal{F}(\rho) \equiv \max_A \frac{F(\rho, A)}{4N} = \frac{1}{2N} \max_A \sum_{i,j=1}^{2^N} \frac{(\pi_i - \pi_j)^2}{(\pi_i + \pi_j)} |\langle i| A |j\rangle|^2 \tag{5.40}$$

, and it has a maximum N for a GHZ state. Meanwhile, using Eq. (5.29) and Eq. (5.30), we can rewrite $\mathcal{I}(\rho)$ (with an extra normalization factor 2 mentioned above) as

$$\mathcal{I}(\rho) = \frac{1}{2N} \max_A \sum_{i,j=1}^{2^N} \frac{(\pi_i - \pi_j)^2}{\sum_k \pi_k^2} |\langle i| A |j\rangle|^2 . \tag{5.41}$$

It is clear that the only difference between $\mathcal{I}(\rho)$ and $\mathcal{F}(\rho)$ is the denominator of the weights of $|\langle i|A|j\rangle|^2$ which are $\sum_k \pi_k^2$ and $\pi_i + \pi_j$, respectively. Note that both $\mathcal{I}(\rho)$ and $\mathcal{F}(\rho)$ are identical to the maximum variance per particle, $\max_A \mathcal{V}(A)/N$, when the quantum state is pure. For general mixed states, however, the difference can be arisen due to the different forms of weights and the operator A which maximizes each measure respectively. We note that quantum Fisher information is the convex roof of the variance, thus it is

a bound for any convex function those are identical to the variance for pure states [97, 106]. However, $\mathcal{I}(\rho)$ for spin states contains purity in the denominator which is necessary for normalization of weights for frequency content, so that the convexity of $\mathcal{I}(\rho)$ is not guaranteed. Therefore, it is not straightforward to compare the two measure analytically Moreover, the difference is very subtle so that only highly mixed states can enlarge it.

5.4 Applications

Example 1– Consider a generalized mixed GHZ state

$$\rho_{\rm G} = \mathcal{N}^{-1}\left(|0\rangle\langle 0|^{\otimes N} + |\epsilon\rangle\langle\epsilon|^{\otimes N} + \gamma\,|0\rangle\langle\epsilon|^{\otimes N} + \gamma\,|\epsilon\rangle\langle 0|^{\otimes N}\right) \tag{5.42}$$

where $|\epsilon\rangle = \cos\epsilon\,|0\rangle + \sin\epsilon\,|1\rangle$ and $\mathcal{N} = 2(1+\gamma\cos^N\epsilon)$. The two components of superposition $|0\rangle^{\otimes N}$ and $|\epsilon\rangle^{\otimes N}$ have an overlap $\langle 0|\epsilon\rangle^N = \cos^N\epsilon$ and their coherence is reduced by a factor γ. For $\gamma = 1$ and $\epsilon = \pi/2$, it is the original GHZ state $\rho_{\rm G} = |{\rm GHZ}\rangle\langle{\rm GHZ}|$ so that the macroscopic quantumness is the maximum N. For a general calculation, one may diagonalize Eq. (5.42) as $\rho_{\rm G} = \gamma_+\,|+\rangle\langle+| + \gamma_-\,|-\rangle\langle-|$, where $|\pm\rangle = \mathcal{N}_\pm^{-1/2}(|0\rangle^{\otimes N} \pm |\epsilon\rangle^{\otimes N})$ with $\mathcal{N}_\pm = 2(1\pm\cos^N\epsilon)$ and $\gamma_\pm = (1\pm\gamma)\mathcal{N}_\pm/2\mathcal{N}$. Then macroscopic quntumness reads,

$$\mathcal{I}(\rho_{\rm G}) \simeq 2\gamma^2/(1+\gamma^2)\epsilon^2 N + O(1), \tag{5.43}$$

where the approximation is only taken in the limit $\epsilon \ll 1$, and γ is still arbitrary. Meanwhile, the quantum Fisher information based measure reads

$$\mathcal{F}(\rho_{\mathrm{G}}) \simeq \gamma^2 \epsilon^2 N + O(1) \tag{5.44}$$

so that the fraction in a high mixture limit is $\mathcal{I}(\rho_{\mathrm{G}})/\mathcal{F}(\rho_{\mathrm{G}}) \simeq 2$ ($\gamma \ll 1$ and $N \gg 1$). Note that when $\gamma = 1$, the state becomes pure $\rho_{\mathrm{G}} = |+\rangle\langle+|$, thus the two measures are identical $\mathcal{I}(\rho_{\mathrm{G}}) = \mathcal{F}(\rho_{\mathrm{G}}) = \max_A \mathcal{V}(A)/N \simeq \epsilon^2 N + O(1)$. This coincides with the result of the original study of the state [90].

Example 2– Suppose now an imperfect generation of GHZ state where we obtain an ideal GHZ state with probability p or a complete mixture otherwise,

$$\rho_{\text{I-GHZ}} = p\,|\text{GHZ}\rangle\langle\text{GHZ}| + (1-p)\frac{I_{2^N \times 2^N}}{2^N}. \tag{5.45}$$

Macroscopic quantumness is found to be

$$\mathcal{I}(\rho_{\text{I-GHZ}}) = p^2 \left(p^2 + 2^{-N}(1-p^2)\right)^{-1} N. \tag{5.46}$$

When $p = 1$ it is $\mathcal{I}_{\text{GHZ}} = N$ indeed, and monotonically decreases as p is lowered, then finally becomes zero at $p = 0$. Thus we confirm that our measure captures the degree of quantum coherence, in terms of the factor p for this

case. Similarly, the quantum Fisher information based measure reads

$$\mathcal{F}(\rho_{\text{I-GHZ}}) = p^2 \left(p + 2^{-(N-1)}(1-p)\right)^{-1} N. \tag{5.47}$$

Once again, we find a difference in scaling factors between $\mathcal{I}$ and $\mathcal{F}$ for a high mixedness limit, $p \ll 1$. The fraction of the two measure for this limit becomes $\mathcal{I}(\rho_{\text{I-GHZ}})/\mathcal{F}(\rho_{\text{I-GHZ}}) \simeq 2$ ($p \ll 1$ and still $N \gg 1$).

Example 3– We present another mixed state that shows sub–optimal precision for quantum metrology [108]

$$\rho_{\text{M}} = \mathcal{C} H_1 \rho_0^{\otimes N} H_1 \mathcal{C} = \frac{1}{2} \begin{pmatrix} \rho_0^{\otimes N-1} & p(\rho_0\sigma_x)^{\otimes N-1} \\ p(\sigma_x\rho_0)^{\otimes N-1} & (\sigma_x\rho_0\sigma_x)^{\otimes N-1} \end{pmatrix}, \tag{5.48}$$

where $\rho_0 = (1+p)/2\,|0\rangle\langle 0| + (1-p)/2\,|1\rangle\langle 1|$. H_1 is Hadamard gate on the first qubit and $\mathcal{C} = \bigotimes_{i=2}^{N} C_{1i}$ where C_{1i} is the controlled-NOT operation with the first qubit being the control and the ith qubit being the target. Calculation of $\mathcal{I}(\rho)$ is straightforward from the explicit form of Eq. (5.48),

$$\mathcal{I}(\rho_{\text{M}}) = 8p^4/(1+p^2)^3 N + O(1) \simeq 8p^4 N + O(1)\ (p \ll 1). \tag{5.49}$$

Meanwhile, we need to identify eigenvalues and eigenvectors of ρ_M to obtain $\mathcal{F}(\rho)$[108] and it reads

$$\mathcal{F}(\rho_{\text{M}}) = p^4 N + O(1). \tag{5.50}$$

We see that the fraction becomes larger than preceding examples

$$\mathcal{I}(\rho_{\mathrm{M}})/\mathcal{F}(\rho_{\mathrm{M}}) \simeq 8 \ (p \ll 1, N \gg 1). \tag{5.51}$$

It is a typical example which shows that computational complexity is much lower for $\mathcal{I}$ than $\mathcal{F}$.

Although $\mathcal{I}$ and $\mathcal{F}$ exhibit different leading factor of N, they both agree that the three examples shown are all macroscopically quantum in certain degrees.

5.5 Quantum phase transition

We have defined a measure of macroscopic quantumness for spin states and verified it by several examples to find it operates properly. In this section, we attempt to search for a natural phenomenon that is genuinely macroscopically quantum. As mentioned in the introduction of this chapter, Debye's law, superconductivity or superfluidity are indeed natural quantum phenomena but they are all accumulations of microscopic quantum effects. For another possible candidate of a genuine macroscopic quantum effect, we investigate a prominent natural quantum phenomenon called quantum phase transition (QPT). QPT is basically that the ground state of a many–body system shows abrupt change of an observable called an order parameter [111]. We review essential properties of the simplest many–body model and apply our measure of macroscopic quantumness for the model.

5.5.1 Quantum phase transition of Ising model

A classical phase transition is the transformation of a physical system due to changing values of thermodynamic parameters such as pressure and temperature. Typically such phases are classified as solid, liquid, or gaseous states. In contrast, quantum phase transition is nothing to do with thermodynamic change. It rather attributes to quantum fluctuation of observables, which is even presence in the zero–temperature states. As a simple and obvious example, we show that 1-d transverse Ising model shows an abrupt change of magnetization when an interaction strength is around the critical point. The Hamiltonian of the transverse Ising model [111, 112] is

$$H_{\text{Ising}}(\lambda) = -\sum_{j=1}^{N} \left(\lambda \sigma_x^{(j)} \sigma_x^{(j+1)} + \sigma_z^{(j)}\right) \tag{5.52}$$

where $\sigma_i^{(j)}$ is i-component Pauli operator on jth site and $\boldsymbol{\sigma}^{(N+1)} \equiv \boldsymbol{\sigma}^{(1)}$ by periodic condition. The exact solution of Eq. (5.52) is well–known [111] and the magnetization of the ground state $\langle \sigma^x \rangle$ can be calculated as

$$\langle \sigma^x \rangle = \begin{cases} 0, & \lambda \leq 1 \\ (1 - \lambda^{-2})^{1/8}, & \lambda > 1 \end{cases} \tag{5.53}$$

and is plotted for changing λ in Fig. 16. For $\lambda < 1$, the ground state is in a disordered paramagnetic phase. In an extreme case $\lambda \ll 1$, the Hamiltonian

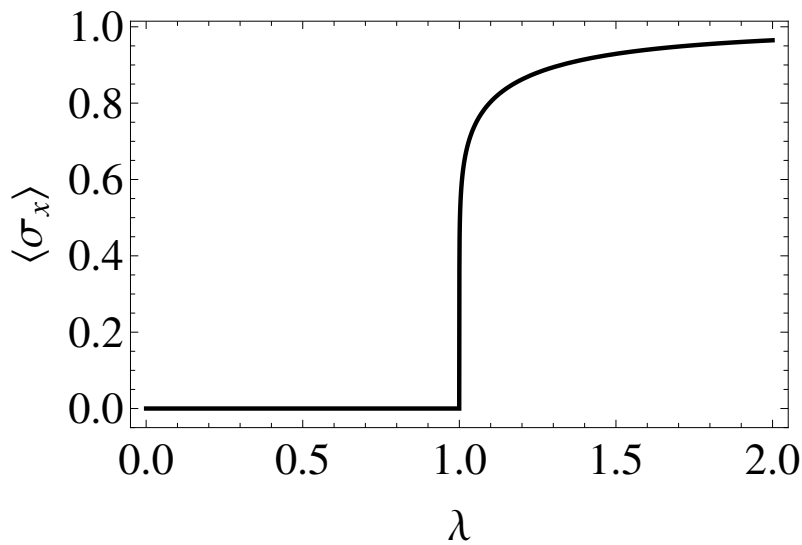

Fig. 16: The magnetization $\langle \sigma^x \rangle$ of the ground state of Ising model versus the interaction strength λ. One can observe an abrupt change of the magnetization near the critical point $\lambda = \lambda_c = 1$.

can be approximately written as

$$H_{\text{Ising}}(\lambda \ll 1) \approx -\sum_{j=1}^{N} \sigma_z^{(j)}, \tag{5.54}$$

so the ground state is found to be $|\uparrow\rangle\,|\uparrow\rangle \ldots |\uparrow\rangle$, which gives the magnetization $\langle \sigma^x \rangle = 0$. Meanwhile, for $\lambda > 1$, the ground state is in an ordered ferromagnetic phase and if $\lambda \gg 1$, the first term in the Hamiltonian becomes dominant as

$$H_{\text{Ising}}(\lambda \gg 1) \approx -\sum_{j=1}^{N} \sigma_x^{(j)} \sigma_x^{(j+1)}. \tag{5.55}$$

In this extreme case, the ground state has two–fold degeneracy due to the global phase flip symmetry. The ground states are $|{\rightarrow}\rangle\,|{\rightarrow}\rangle\ldots|{\rightarrow}\rangle$ and $|{\leftarrow}\rangle\,|{\leftarrow}\rangle\ldots|{\leftarrow}\rangle$, where $|{\rightarrow}\rangle = (|{\uparrow}\rangle + |{\downarrow}\rangle)/\sqrt{2}$ and $|{\leftarrow}\rangle = (|{\uparrow}\rangle - |{\downarrow}\rangle)/\sqrt{2}$.

Near the critical point $\lambda_c = \lambda = 1$, the global phase flip symmetry of the ground state is broken [111] and an abrupt change of the magnetization occurs. This is the phenomenon called QPT; phase transition of a bulk matter due to quantum mechanical fluctuations.

5.5.2 Macroscopic quantumness of quantum phase transition

Firstly, we consider the thermodynamic limit of the model (*i.e.* $N \to \infty$) and take a partial block of L contiguous spins to obtain the reduced density matrix ρ_L. Then we calculate $\mathcal{I}(\rho_L)$ of the block and watch how it behaves for the different values of the initial interaction strength λ. Note that ρ_L is generally not a pure state since L spins are originally correlated with the rest part of the spin chain. Even if we consider the ground state of the entire spins, the mixedness occurs due to the two-fold degeneracy for $\lambda > 1$, which originates in the global phase flip symmetry [111]. Such an inevitable mixedness makes other existing measures, especially only for pure state [89, 90, 91, 92, 95, 96] not applicable to this study. We numerically obtain

$$\mathcal{I}(\rho_L) = \max_{A} \frac{\mathrm{Tr}[\rho_L^2 A^2 - \rho_L A \rho_L A]}{L\mathrm{Tr}[\rho_L^2]} \tag{5.56}$$

for L upto 12 as depicted in Fig. 17. The details of calculations is as follows. The Hamiltonian of Ising model can be diagonalized a well known operator transformations. Suppose, two Majorana operators for each site l of the N spins,

$$c_{2l} \equiv \left(\prod_{m=0}^{l-1} \sigma_m^z \right) \sigma_l^x; \qquad c_{2l+1} \equiv \left(\prod_{m=0}^{l-1} \sigma_m^z \right) \sigma_l^y. \tag{5.57}$$

Note that c_m are Hermitian operators and satisfy the anticommutation relation

$$\{c_m, c_n\} = 2\delta_{mn}. \tag{5.58}$$

It is known that the expectation values $\langle c_m c_n \rangle = \delta_{mn} + i\Gamma_{mn}$ completely characterize L block of the ground state. Matrix Γ reads

$$\Gamma = \begin{bmatrix} \Pi_0 & \Pi_1 & \cdots & \Pi_{L-1} \\ \Pi_{-1} & \Pi_0 & & \vdots \\ \vdots & & \ddots & \vdots \\ \Pi_{1-L} & \cdots & \cdots & \Pi_0 \end{bmatrix},$$

$$\Pi_l = \begin{bmatrix} 0 & g_l \\ -g_{-l} & 0 \end{bmatrix}, \tag{5.59}$$

where g_l is given by

$$g_l = \frac{1}{2\pi} \int_0^{2\pi} d\phi \, e^{-il\phi} \frac{\lambda e^{-i\phi} - 1}{|\lambda e^{-i\phi} - 1|} \tag{5.60}$$

Since Γ is a skew-symmetric matrix, we can find an orthogonal matrix $V \in \mathrm{SO}(2L)$ that block-diagonalizes Γ into

$$\tilde{\Gamma} = V\Gamma V^T = \oplus_{m=0}^{L-1}\nu_m \begin{bmatrix} 0 & 1 \\ -1 & 0 \end{bmatrix} \tag{5.61}$$

Then, the set of $2L$ Majorana operators $d_m = \sum_{n=0}^{2L-1} V_{mn}c_n$ have a block-diagonal correlation matirx $\langle d_m d_n = \delta_{mn} + i\tilde{\Gamma}_{mn}\rangle$. Now, L fermionic operators $b_l \equiv (d_{2l} + id_{2l+1})/2$ obeying $\{b_m, b_n\} = 0$ and $\{b_m^\dagger b_n\} = \delta_{mn}$ have expectation values

$$\langle b_m\rangle = 0, \qquad \langle b_m b_n\rangle = 0, \qquad \langle b_m^\dagger b_n\rangle = \delta_{mn}\frac{1+\nu_m}{2}. \tag{5.62}$$

This indicates that the mixed states of the block L can be described as a product sate in b_m basis as

$$\rho = \bigotimes_{m=0}^{L-1} \rho_m. \tag{5.63}$$

However, when we express the operator A of $\mathcal{I}(\rho) = \mathcal{P}^{-1}\max_A \mathrm{Tr}[\rho^2 A^2 - \rho A\rho A]$ using the operators b_m, it becomes nonlocal over the different modes of b_m which complicates the calculation of $\mathcal{I}(\rho)$. Thus, we alternatively re-express Eq. (5.63) by Pauli operator basis. From Eq. (5.62), one can find

$$\rho_m = \frac{1-\nu_m}{2} b_m b_m^\dagger + \frac{1+\nu_m}{2} b_m^\dagger b_m. \tag{5.64}$$

and using Eq. (5.57),

$$
\begin{aligned}
b_m &= \frac{1}{2}(d_{2l} + id_{2l+1}) = \frac{1}{2}\sum_{n=0}^{2L-1}\left(V_{2l,n}c_n + iV_{2l+1,n}c_n\right) \\
&= \frac{1}{2}\Big[\sum_{k=0}^{L-1}\left(V_{2l,2k} + iV_{2l+1,2k}\right)c_{2k} \\
&\qquad + \sum_{k=0}^{L-1}\left(V_{2l,2k+1} + iV_{2l+1,2k+1}\right)c_{2k+1}\Big] \\
&= \frac{1}{2}\Bigg[\sum_{k=0}^{L-1}\left(V_{2l,2k} + iV_{2l+1,2k}\right)\left(\prod_{m=0}^{k-1}\sigma_m^z\right)\sigma_l^x \\
&\quad + \sum_{k=0}^{L-1}\left(V_{2l,2k+1} + iV_{2l+1,2k+1}\right)\left(\prod_{m=0}^{k-1}\sigma_m^z\right)\sigma_l^y\Bigg]
\end{aligned}
\tag{5.65}
$$

We now have an analytic form of $\mathcal{I}(\rho)$ since ρ and $A = \sum_{j=1}^{N}\boldsymbol{\alpha}^{(j)}\cdot\boldsymbol{\sigma}^{(j)}$ are written in Pauli basis. However, the measure requires maximization over the operator A or the local unit vectors $\boldsymbol{\alpha}^{(j)}$s. Since this multi-dimensional optimization cannot be done analytically, we obtain the final values of $\mathcal{I}(\rho)$ by numerical methods.

We are not required to analyze the eigenvalues and vectors of ρ_L, which is a great benefit of the measure in terms of computational complexity. Nevertheless, a difficulty of increasing the value of L mainly comes from maximization procedure of L independent local parameters of operators, since the block ρ_L has no translational symmetry due to the open boundaries. One can

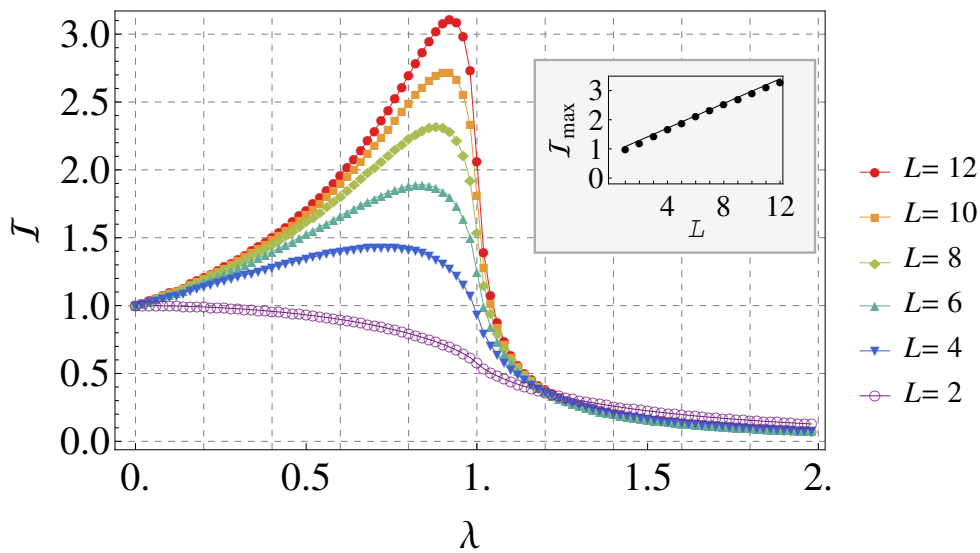

Fig. 17: Macroscopic quantumness of a block of L partial spins $\mathcal{I}(\rho_L(\lambda))$ versus the interaction strength of Ising model λ. (Inset) Black dots are the maximal values of $\mathcal{I}(\rho_L)$ for a block L. The red line is a linear fit, $\max_\lambda \mathcal{I}(\rho_L(\lambda)) \simeq 0.21L + O(1)$

observe a tendency that $\mathcal{I}(\rho_L)$ peaks right before the critical point $\lambda_c = 1$ and rapidly decreases as the interaction becomes stronger. Such a character becomes more clear as we investigate a larger block L of spins. Furthermore, if we collect the maximum values of $\mathcal{I}(\rho_L)$ of each block L, it exhibit a linear scaling such that $\max_\lambda \mathcal{I}(\rho_L(\lambda)) \simeq 0.21L + O(1)$ as shown in the inset of Fig. 17. Thus, for any large value of L, the system may possess a degree of macroscopic quantumness proportional to the system size at the critical point. It is mainly because spins acquire long-range correlations near the critical point [112]. In that sense, QPT maybe regarded as a genuine macroscopic quantum phenomenon where a subset of the system cannot explains the entire quantum mechanical properties, in contrast to superconductivity or superfluidity, [34].

5.6 Remarks

We classified various quantum effects into three main categories. One is typical microscopic quantum effects such as quantization of microscopic energy levels or superposition of a single or a small number of particle states. When such microscopic quantum effects are accumulated to constitute a bulk effect in macroscopic scale, people called it a macroscopic quantum effect. However, there have been arguments on this issue [33, 34] and such an accumulation of microscopic quantum effects should be discriminated from genuine macroscopic quantum effects. One well–established genuine macro-

scopic quantum effect is quantum metrology, where we can estimate an unknown parameter of a physical system over the classical limit by using a quantumly correlated probe state [33, 37]. Since such an enhancement cannot be achieved by a fractional part of the total probe state, it is not a cumulative quantum effect, which in other words a genuine macroscopic quantum effect [33]. We reviewed a measure of macroscopic quantumness for bosonic states, which counts oscillations of interference fringes in phase space illustration [30]. We extended such a concept to multiple spin states and proposed a measure of macroscopic quantumness by investigating spin Wigner functions for different forms of states including mixtures. We verified the measure works for typical and intuitive macroscopic quantum states. We finally applied the measure to a well–known quantum phenomena called quantum phase transition. Remarkably, the degree of macroscopic quantumness becomes large near the critical point of the system parameter where quantum phase transition occurs. Furthermore, the maximal values of each finite number of spins increase in a linear manner to the system size. This indicates that the system still can be macroscopically quantum even when the system is arbitrarily large, say a Avogadro's number ($\approx 10^{23}$). This arguably can be concluded that Schrödinger's cat exist in nature.

Chapter 6

Conclusion

Firstly, we have reviewed several well–known quantum effects and clarify a hierarchy of them in terms of emergence of such effects in macroscopic levels. The basic building block is microscopic quantum effects, where non–classical effects emerge in atomic length scales. Such effects can be accumulated upto macroscopic length scales, still being described by atomic–level interactions. Typical examples of them are superconductivity, superfluidity, and Debye's T^3 law. We call a phenomenon a genuine macroscopic quantum effect if it occurs in a macroscopic scale, yet cannot be described or explained by a subset of the entire system. One famous example of such kind is Schrödinger's cat, where two macroscopically distinct states of a cat, alive and dead, is in a form of quantum superposition. It is not an accumulation of microscopic quantum effects, since any local part of a cat cannot completely describe the superposition; we lose an amount of the initial information when we discard other parts. For a more practical example, we dealt with quantum parameter estimation, where the task is to estimate an unknown parameter of a black–boxed material with a probing quantum state. The precision of the estimation is improved over the classical limit, and we can not achieve the same

level of improved precision when we lose a single part of the original state. This is because the probing quantum state is initially highly correlated so that the information each local part acquires from the unknown target material is transported and shared by the entire system. In that manner, it is an apparent genuine macroscopic quantum effect by definition.

In subsequent chapters, we proposed generation schemes of macroscopic entanglement. We first conducted general investigation on entanglement generation for atomic energy levels and optical thermal states. We then extended the study to entanglement between a single–photon superposition and thermal states, and even further to direct interaction between two thermal states. Throughout the study we found a common tendency that the temperature of the thermal state is not a critical factor for entanglement generation; entanglement is generated even for the infinite temperature limit for most cases. What more critical is coherent and strong interactions those are sensitive to the microscopic quantum states.

We also proposed a scheme for a hybrid entanglement generation for optical systems utilizing a photon addition technique. The basic idea is that adding a single photon into an ideal coherent state yields another approximate coherent state with a larger amplitude. We identify such a behavior as an amplification process. We rigorously found the optimal amplification gain and the fidelity in mathematical terms. Since the photon addition event can be heralded by a triggering detection, we could generate a hybrid entanglement from a product of a vacuum and a coherent state by mixing two heralding

parts.

Besides of generation ideas for macroscopic quantum states, we also proposed a criterion for quantifying the degree of macroscopic quantumness for arbitrary quantum states. We reviewed a measure of macroscopic quantumness for optical systems, and extend the essential idea to spin systems. We identified typical behaviors of interference fringes in phase space of macroscopic quantum states of spins, then defined a measure by capturing the structures of them. We proved that our measure is equivalent to a decay rate of system purity under a Lindblad type of decoherence process. We applied the measure to several examples and verified that the measure works in an intuitive manner. We further investigated macroscopic quantumness of a many–body spin system, when the system undergoes quantum phase transition. Remarkably, the system becomes highly macroscopic quantum near the critical point, where quantum phase transition occurs. Moreover, the maximum value of macroscopic quantumness increases in a linear manner to the system size, indicating that even a macroscopic–scaled system (say an Avogadro number of spins) can exhibit a high degree of macroscopic quantumess as well. We argued that quantum phase transition is a naturally occurring genuine macroscopic quantum phenomenon that coincides with the original Schrödinger's argument.

Bibliography

[1] D. J. Griffith, *Introduction to Quantum Mechanics*, Pearson Prentice Hall (2004).

[2] E. Schrödinger, "Die gegenwrtige situation in der quantenmechanik," Naturwissenschaften **23**, 807 (1935).

[3] C. Monroe, D. M. Meekhof, B. E. King and D. J. Wineland, "A 'Schrödinger cat' superposition state of an atom," Science **272**, 1131 (1996).

[4] M. Arndt, O. Nairz, J. Vos-Andreae, C. Keller, G. van der Zouw, and A. Zeilinger, "Wave-particle duality of C60 molecules," Nature **401**, 680 (1999).

[5] C. H. van der Wal, A. C. J. ter Haar, F. K. Wilhelm, R. N. Schouten, C. J. P. M. Harmans, T. P. Orlando, Seth Lloyd, J. E. Mooij, "Quantum Superposition of Macroscopic Persistent-Current States," Science **290**, 773 (2000).

[6] J. R. Friedman, V. Patel, W. Chen, S. K. Tolpygo, and J. E. Lukens, "Quantum superposition of distinct macroscopic states," Nature **406**, 43 (2000).

[7] A. Ourjoumtsev, H. Jeong, R. Tualle-Brouri, and P. Grangier, "Generation of optical 'Schrödinger cats' from photon number states," Nature **448**, 784 (2007).

[8] M. Brune, E. Hagley, J. Dreyer, X. Matre, A. Maali, C. Wunderlich, J.M. Raimond, S. Haroche, "Observing the progressive decoherence of the 'meter' in a quantum measurement," Phys. Rev. Lett. **77**, 4887 (1996).

[9] S. Delglise, I. Dotsenko, C. Sayrin, J. Bernu, M. Brune, J.-M. Raimond, S. Haroche, "Reconstruction of non-classical cavity field states with snapshots of their decoherence," Nature **455**, 510 (2008).

[10] W.-B. Gao, C.-Y. Lu, X.-C. Yao, P. Xu, O. Guhne, A. Goebel, Y.-A. Chen, C.-Z. Peng, Z.-B. Chen, and J.-W. Pan, "Experimental demonstration of a hyper-entangled ten-qubit Schrödinger cat state," Nat. Phys. **6**, 331 (2010).

[11] I. Afek, O. Ambar, and Y. Silberberg, "High-NOON states by mixing quantum and classical light," Science **328**, 879 (2010).

[12] M. Arndt and K. Hornberger, "Testing the limits of quantum mechanical superpositions," Nat. Phys. **10**, 271 (2014).

[13] T.Sh. Iskhakov, I.N. Agafonov, M.V. Chekhova, G.O. Rytikov, G. Leuchs, "Polarization properties of macroscopic Bell states," Phys. Rev. A **84**, 045804 (2011).

[14] T.Sh. Iskhakov, M.V. Chekhova, G.O. Rytikov, G. Leuchs, "Macroscopic pure state of light free of polarization noise," Phys. Rev. Lett. **106**, 113602 (2011).

[15] T.Sh. Iskhakov, I.N. Agafonov, M.V. Chekhova, G. Leuchs, "Polarization-entangled light pulses of 10^5 photons," Phys. Rev. Lett. **109**, 150502 (2012).

[16] B. Kanseri, T.Sh. Iskhakov, G. Rytikov, M.V. Chekhova, G. Leuchs, "Multiphoton nonclassical correlations in entangled squeezed vacuum states," Phys. Rev. A **87**, 032110 (2013).

[17] F.D. Martini, F. Sciarrino, C. Vitelli, "Entanglement test on a microscopic-macroscopic system," Phys. Rev. Lett. **100**, 253601 (2008).

[18] F. De Martini, "Amplification of quantum entanglement," Phys. Rev. Lett. **81**, 2842 (1998).

[19] F. De Martini, "Quantum superposition of parametrically amplified multiphoton pure states," Phys. Lett. A **250**, 15 (1998).

[20] D.M. Greenberger, M.A. Horne, A. Zeilinger, *Bells Theorem, Quantum Theory, and Conceptions of the Universe*, Kluwer Academics, Dordrecht, pp. 7376 (1989).

[21] D. Bouwmeester, J.-W. Pan, M. Daniell, H. Weinfurter, A. Zeilinger, "Observation of three-photon Greenberger-Horne-Zeilinger entanglement," Phys. Rev. Lett. **82**, 1345 (1999).

[22] Z. Zhao, Y.-A. Chen, A.-N. Zhang, T. Yang, H.J. Briegel, J.-W. Pan, "Experimental demonstration of five-photon entanglement and open-destination teleportation," Nature **430** 54, (2004).

[23] Y.-F. Huang, B.-H. Liu, L. Peng, Y.-H. Li, L. Li, C.-F. Li, G.-C. Guo, "Experimental generation of an eight-photon Greenberger-HorneZeilinger state," Nat. Commun. **2** 546, (2011).

[24] B. Sanders, "Quantum dynamics of the nonlinear rotator and the effects of continual spin measurement," Phys. Rev. A **40**, 2417 (1989).

[25] A.N. Boto, P. Kok, D.S. Abrams, S.L. Braunstein, C.P. Williams, J.P. Dowling, "Quantum interferometric optical lithography: exploiting entanglement to beat the diffraction limit," Phys. Rev. Lett. **85**, 2733 (2000).

[26] P. Kok, H. Lee, J.P. Dowling, "Creation of large-photon-number path entanglement conditioned on photodetection,"Phys. Rev. A **65**, 052104 (2002).

[27] I. Afek, O. Ambar, Y. Silberberg, "High-NOON states by mixing quantum and classical light," Science **328**, 879 (2010).

[28] N. Bruno, A. Martin, P. Sekatski, N. Sangouard, R.T. Thew, N. Gisin, "Displacement of entanglement back and forth between the micro and macro domains,"Nat. Phys. **9**, 545 (2013).

[29] A.I. Lvovsky, R. Ghobadi, A. Chandra, A.S. Prasad, C. Simon, "Observation of micromacro entanglement of light," Nat. Phys. **9** 541 (2013).

[30] C.-W. Lee and H. Jeong, "Quantification of macroscopic quantum superpositions within phase space," Phys. Rev. Lett. **106**, 220401 (2011).

[31] M. Planck, *The Theory of Heat Radiation.*, M. Masius, (transl.) (2nd ed.). P. Blakiston's Son & Co. OL 7154661M (1914).

[32] L. N. Cooper, "Bound electron pairs in a degenerate Fermi gas," Phys. Rev. **104** (4), 11891190 (1956).

[33] F. Fröwis and W. Dür, "Measures of macroscopicity for quantum spin systems," New J. Phys. **14**, 093039 (2012).

[34] A. J. Leggett, "Macroscopic quantum systems and the quantum theory of measurement," Prog. Theor. Phys. Suppl. **69**, 80 (1980).

[35] J. P. Dowling, "Quantum optical metrology the lowdown on high-N00N states," Contemp. Phys. **49**, 125 (2008).

[36] V. Giovannetti, S. Lloyd and L. Maccone, "Quantum metrology," Phys. Rev. Lett. **96**, 010401 (2006).

[37] J. Joo, W. J. Munro, and T. P. Spiller, "Quantum metrology with entangled coherent states," Phys. Rev. Lett. **107**, 083601 (2011).

[38] S. L. Braunstein and C. M. Caves, "Statistical distance and the geometry of quantum states," Phys. Rev. Lett. **72**, 3439 (1994)

[39] S. L. Braunstein, C. M. Caves, and G. J. Milburn, "Generalized uncertainty relations: theory, examples, and Lorentz invariance," Ann. Phys. (N.Y.) **247**, 135 (1996).

[40] A. Einstein, B. Podolsky, and N. Rosen, "Can quantum-mechanical description of physical reality be considered complete?," Phys. Rev. **47**, 777 (1935).

[41] R. Horodecki, P. Horodecki, M. Horodecki and K. Horodecki, "Quantum entanglement," Rev. Mod.Phys. **81**, 865 (2009).

[42] R. F. Werner, "Quantum states with Einstein-Podolsky-Rosen correlations admitting a hidden-variable model," Phys. Rev. A **40**, 4277 (1989).

[43] A. Peres, "Separability criterion for density matrices," Phys. Rev. Lett. **77**, 1413 (1996).

[44] M. Horodecki, P. Horodecki, and R. Horodecki, "Separability of mixed states: necessary and sufficient conditions," Phys. Lett. A **223**, 1 (1996).

[45] J. Lee, M. S. Kim, Y. J. Park, and S. Lee, "Partial teleportation of entanglement in a noisy environment," J. Mod. Opt. **47**, 12 (2000).

[46] E. C. G. Sudarshan, "Equivalence of semiclassical and quantum mechanical descriptions of statistical light beams," Phys. Rev. Lett. **10**, 277 (1963).

[47] M. S. Kim, W. Son, V. Bužek, and P. L. Knight, "Entanglement by a beam splitter: Nonclassicality as a prerequisite for entanglement," Phys. Rev. A **65**, 032323 (2002).

[48] R. Filip, M. Dušek, J. Fiurášek, and L. Mišta, "Bell-inequality violation with 'thermal' radiation," Phys. Rev. A **65**, 043802 (2002).

[49] S. Bose, I. Fuentes-Guridi, P. L. Knight, and V. Vedral, "Subsystem purity as an enforcer of entanglement," Phys. Rev. Lett. **87**, 050401 (2001).

[50] M. S. Kim, J. Lee, D. Ahn, and P. L. Knight, "Entanglement induced by a single-mode heat environment," Phys. Rev. A **65**, 040101(R) (2002).

[51] A. Ferreira, A. Guerreiro, V. Vedral, "Macroscopic thermal entanglement due to radiation pressure," Phys. Rev. Lett. **96**, 060407 (2006).

[52] H. Jeong and T. C. Ralph, "Transfer of nonclassical properties from a microscopic superposition to macroscopic thermal states in the high temperature limit," Phys. Rev. Lett. **97**, 100401 (2006).

[53] H. Jeong and T. C. Ralph, "Quantum superpositions and entanglement of thermal states at high temperatures and their applications to quantum-information processing," Phys. Rev. A **76**, 042103 (2007).

[54] H. Jeong, M. Paternostro, and T. C. Ralph, "Failure of local realism revealed by extremely-coarse-grained measurements," Phys. Rev. Lett. **102**, 060403 (2009).

[55] M. Paternostro, H. Jeong, and M. S. Kim, "Entanglement of mixed macroscopic superpositions: an entangling-power study," Phys. Rev. A **73**, 012338 (2006).

[56] J. H. Shapiro and M. Razavi, "Continuous-time cross-phase modulation and quantum computation," New J. Phys. **9**, 16 (2007).

[57] B. He, Q. Lin, and C. Simon, "Cross-Kerr nonlinearity between continuous-mode coherent states and single photons," Phys. Rev. A **83**, 053826 (2011).

[58] G. McKeown, F.L. Semião, H. Jeong, and M. Paternostro, "Genuine multipartite nonlocality of entangled thermal states," Phy. Rev. A **82**, 022315 (2010).

[59] N. B. An and T. T. Hoa, "Generation of free-traveling four-mode cluster-type entangled coherent states," Phys. Lett. A **373**, 2601 (2009).

[60] S. M. Barnett and P. M. Radmore, *Methods in Theoretical Quantum Optics*, Clarendon Press, Oxford (1997).

[61] R. J. Glauber, "Coherent and incoherent states of the radiation field," Phys. Rev. **131**, 27662788 (1963).

[62] K. Kreis and P. van Loock, "Classifying, quantifying, and witnessing qudit-qumode hybrid entanglement," Phys. Rev. A **85**, 032307 (2012).

[63] A. Furusawa, P. van Loock, *Quantum Teleportation and Entanglement: A Hybrid Approach to Optical Quantum Information Processing*, John Wiley and Sons, New York (2011).

[64] P. van Loock, "Optical hybrid approaches to quantum information," Laser Photon. Rev. **5**, 167 (2011).

[65] K. Park, S.-W. Lee, H. Jeong, "Quantum teleportation between particle-like and fieldlike qubits using hybrid entanglement under decoherence effects," Phys. Rev. A **86**, 062301 (2012).

[66] J. Rigas, O. Ghne, N. Ltkenhaus, "Entanglement verification for quantum-key-distribution systems with an underlying bipartite qubit-mode structure," Phys. Rev. A **73**, 012341 (2006).

[67] C. Wittmann, J. Frst, C. Wiechers, D. Elser, H. Hseler, N. Ltkenhaus, G. Leuchs, "Witnessing effective entanglement over a 2 km fiber channel," Opt. Express **18**, 4499 (2010).

[68] S.-W. Lee and H. Jeong, "Near-deterministic quantum teleportation and resource-efficient quantum computation using linear optics and hybrid qubits," Phys. Rev. A **87**, 022326 (2013).

[69] H. Kwon, H. Jeong, "Violation of the BellClauser-Horne-Shimony-Holt inequality using imperfect photodetectors with optical hybrid states," Phys. Rev. A **88**, 052127 (2013).

[70] N. Spagnolo, C. Vitelli, M. Paternostro, F. De Martini, F. Sciarrino, "Hybrid methods for witnessing entanglement in a microscopic-macroscopic system," Phys. Rev. A **84**, 032102 (2011).

[71] M. Stobiska, P. Sekatski, A. Buraczewski, N. Gisin, G. Leuchs, "Bell-inequality tests with macroscopic entangled states of light," Phys. Rev. A **84**, 034104 (2011).

[72] M. Stobiska, F. Tppel, P. Sekatski, A. Buraczewski, "Towards loophole-free Bell inequality test with preselected unsymmetrical singlet states of light," Phys. Rev. A **89** 022119 (2014).

[73] J. S. Bell, "On the problem of hidden variables in quantum mechanics," Rev. Mod. Phys. **38**, 447452 (1966).

[74] P. M. Pearle, "Hidden-variable example based upon data rejection," Phys. Rev. D **2**, 14181425 (1970).

[75] C. Gerry,"Generation of optical macroscopic quantum superposition states via state reduction with a Mach-Zehnder interferometer containing a Kerr medium," Phys. Rev. A **59**, 4095–4098 (1999).

[76] K. Nemoto and W. J. Munro, "Nearly deterministic linear optical controlled-NOT gate," Phys. Rev. Lett. **93**, 250502 (2004).

[77] H. Jeong, "Using weak nonlinearity under decoherence for macroscopic entanglement generation and quantum computation," Phys. Rev. A **72**, 034305 (2005).

[78] W. J. Munro, K. Nemoto, and T. P. Spiller, "Weak nonlinearities: a new route to optical quantum computation," New J. Phys. **7**, 137 (2005).

[79] M. Hosseini, S. Rebić, B. M. Sparkes, J. Twamley, B. C. Buchler, and P. K. Lam, "Memory-enhanced noiseless cross phase modulation," arXiv:1112.2010.

[80] J. H. Shapiro, "Single-photon Kerr nonlinearities do not help quantum computation," Phys. Rev. A **73**, 062305 (2006).

[81] J. Gea-Banacloche, "Impossibility of large phase shifts via the giant Kerr effect with single-photon wave packets," Phys. Rev. A **81**, 043823 (2010).

[82] A. Zavatta, S. Viciani and M. Bellini, "Quantum-to-classical transition with single-photon-added coherent states of light," Science **306**, 660662 (2004).

[83] V. Parigi, A. Zavatta, "Probing quantum commutation rules by addition and subtraction of single photons to/from a light field," M. S. Kim and M. Bellini, Science **317**, 1890 (2007).

[84] A. Zavatta, V. Parigi, M. S. Kim, H. Jeong, and M. Bellini, "Experimental demonstration of the bosonic commutation relation via superpositions of quantum operations on thermal light fields," Phys. Rev. Lett. **103**, 140406 (2009)

[85] A. Lamas–Linares, C. Simon, J. C. Howell, and D. Bouwmeester, "Experimental quantum cloning of single photons," Science **296**, 712-714 (2002).

[86] H. Jeong, A. Zavatta, M. Kang, S.-W. Lee, L. S. Costanzo, S. Grandi, T. C. Ralph, and M. Bellini, "Generation of hybrid entanglement of light," Nat. Photon. **8**, 564 (2014).

[87] O. Morin, K. Haung, J. Liu, H.L. Jeannic, C. Fabre, J. Laurat, "Remote creation of hybrid entanglement between particle-like and wave-like optical qubits," Nat. Photon. **8**, 570 (2014).

[88] A. J. Leggett, "Testing the limits of quantum mechanics: motivation, state of play, prospects," J. Phys.: Condens. Matter **14**, R415 (2002).

[89] J. I. Korsbakken, K. B. Whaley, J. Dubois, and J. I. Cirac, "Measurement-based measure of the size of macroscopic quantum superpositions," Phys. Rev. A **75**, 042106 (2007).

[90] W. Dür, C. Simon, and J. I. Cirac, "Effective size of certain macroscopic quantum superpositions," Phys. Rev. Lett. **89**, 210402 (2002).

[91] A. Shimizu and T. Miyadera, "Stability of quantum states of finite macroscopic systems against classical noises, perturbations from environments, and local neasurements," Phys. Rev. Lett. **89**, 270403 (2002).

[92] G. Björk and P. G. L. Mana, "A size criterion for macroscopic superposition states," J. Opt. B **6**, 429 (2004).

[93] A. Shimizu and T. Morimae, "Detection of macroscopic entanglement by correlation of local observables," Phys. Rev. Lett. **95**, 090401 (2005).

[94] E. G. Cavalcanti and M. D. Reid, "Signatures for generalized macroscopic superpositions," Phys. Rev. Lett. **97**, 170405 (2006).

[95] F. Marquardt, B. Abel, and J von Delft, "Measuring the size of a quantum superposition of many-body states," Phys. Rev. A **78**, 012109 (2008).

[96] P. Sekatski, N. Sangouard, N. Gisin, "Size of quantum superpositions as measured with classical detectors," Phys. Rev. A **89**, 012116 (2014).

[97] F. Fröwis, N. Sangouard and N. Gisin, Optics Communications, "Linking measures for macroscopic quantum states via photon-spin mapping," http://dx.doi.org/10.1016/j.optcom.2014.07.017 (2014).

[98] T. Baumgratz, M. Cramer, and M.B. Plenio, "Quantifying coherence," Phys. Rev. Lett. **113**, 140401 (2014).

[99] D. Girolami, "Observable measure of quantum coherence in finite dimensional systems," Phys. Rev. Lett. **113**, 170401 (2014)

[100] Y. Y. Xu, "A unified measure of macroscopic quantum superposition," Phys. Scr. **88**, 055005 (2013)

[101] A. Laghaout, J. S. Neergaard-Nielsen, and U. L. Andersen, "Assessments of macroscopicity for quantum optical states," Optics Communications, http://dx.doi.org/10.1016/j.optcom.2014.07.046 (2014)

[102] S. Nimmrichter, K. Hornberger, "Macroscopicity of mechanical quantum superposition states," Phys. Rev. Lett. **110**, 160403 (2013).

[103] H. Jeong, M. Kang and H. Kwon, "Characterizations and quantifications of macroscopic quantumness and its implementations using optical fields," Optics Communications, http://dx.doi.org/10.1016/j.optcom.2014.07.012 (2014).

[104] D. F. Walls and G. J. Milburn, *Quantum Optics*, Springer (1994).

[105] W. H. Louisell, *Quantum Statistical Properties of Radiation*, Wiley (1973).

[106] S. Yu, "Quantum fisher information as the convex roof of variance," arXiv:1302.5311 (2013).

[107] Y. P. Kalmykov, W. T. Coffey and S. V. Titov, "Master equation in phase space for a spin in an arbitrarily directed uniform external field," J. Stat. Phys. **131** 969 (2008).

[108] K. Modi, H. Cable, M. Williamson and V. Vedral, "Quantum correlations in mixed-state metrology," Phys. Rev. X **1**, 021022 (2011).

[109] A. B. Klimov and S. M. Chumakov, *A Group-Theoretical Approach to Quantum Optics* (WILEY-VCH Verlag GmbH & Co. KGaA, Weinheim, 2009)

[110] T. Morimae, "Superposition of macroscopically distinct states means large multipartite entanglement," Phys. Rev. A **81**, 010101(R) (2010).

[111] T. J. Osborne and M. A. Nielsen, "Entanglement in a simple quantum phase transition," Phys. Rev. A **66**, 032110 (2002).

[112] G. Vidal, J. I. Latorre, E. Rico and A. Kitaev, "Entanglement in Quantum Critical Phenomena," Phys. Rev. Lett. **90**, 227902 (2003).

국문초록

양자역학(量子力學)은 지난 백여 년에 걸쳐 고전 물리학이 설명하지 못했던 원자(原子), 광자(光子)와 같은 미시(微視) 물리계의 현상들을 성공적으로 기술하고 예측해왔다. 한편, 그러한 양자역학적 효과들이 우리가 살고 있는 거시(巨視)세계에서도 여전히 발현될 수 있는지에 대한 여부는 자명하지 않았다. 그에 대한 극명한 예로서, 슈뢰딩거의 고양이 사고(思考)실험을 들 수 있다. 이는, 양자역학이 특별히 미시계에만 적용되는 법칙이 아니라면, 거시적으로 확연히 구분되는 고양이의 살아있거나 죽어있는 상태 또한 양자역학적인 중첩상태에 있을 수 있음을 이야기한다. 그러나 우리는 현실에서 그토록 비직관적인 고양이의 상태를 관측한 적이 없으며 이러한 이유로 거시세계에서의 양자역학적 효과에 대한 의문은 계속 이어져왔다.

우리는 이러한 의문에 대한 실마리로서, 고양이 대신 실험적으로 접근성이 높은 빛의 열(熱)적상태를 이용하여 미시적 원자와 양자 얽힘을 생성할 수 있음을 밝혔다. 열적상태란 높은 온도의 물체에서 방사되는 빛과 같은데 용광로속의 쇳물이 내는 붉은 계열의 빛도 열적상태의 일종이다. 열적상태는 고양이와 같이 매우 고전물리적인 특성을 가지고 있고 사람의 눈으로 관측할 수 있으므로 빛의 고양이 상태로 여길 수 있다. 따라서 매우 높은 온도를 갖는 열적상태에서 양자 얽힘을 만들어낸것은, 거시세계의 물체에도 특정한 상호작용을 가한다면 충분히 양자역학적 효과를 이끌어낼 수 있음을 의미한다.

또 다른 빛의 상태 중 고양이에 비유될 수 있는 것으로 결맞음 상태가 있다. 결맞음 상태는 레이저에서 나오는 빛으로 볼 수 있으며 역시 거시적으로 구분 가능한 고전적 빛이다. 우리는 주어진 빛의 상태에 광자 하나를 추가하는 특별한 실험적인 방법을 이용하여 결맞음 상태와 미시적인 광자상태간의 양자 얽힘을 생성하는 방법을 제안하였다. 이는 기존의 방법들과 달리 비선형물질을 직접적으로 사용하지 않기때문에 실험적인 접근성이 매우 높다. 우리의 이론적 제안은 최근 실험적으로도 구현되었으며 실질적 양자효과 활용에 큰 도움을 준다.

여러 연구자들은 다양한 물리계를 이용하여 슈뢰딩거 고양이 상태와 같은 거시적 양자 중첩을 구현하려는 시도를 해왔다. 그러나 이용된 물리계의 특성들이 서로 다르고 양자 상태의 수학적 형태가 또한 판이하여 그들의 거시적 양자성을 서로 비교하는 것은 실질적으로 불가능하였다. 그러나 최근 위상공간상의 간섭무늬 모양을 이용한 거시적 양자성의 척도가 제안되었고, 우리는 이를 원자의 스핀계에 대해 확장하여 정립하였다. 우리는 고안된 척도를 자연적으로 일어나는 중요한 양자 현상중 하나인 '양자 상전이(量子 相轉移)'에 대해 적용하고 분석하였다. 그 결과, '양자 상전이'는 슈뢰딩거의 고양이에 해당하는 높은 거시적 양자 중첩의 척도를 보였고, 이는 매우 큰 물리계에도 해당되어 거시계에서도 진정한 의미의 양자역학적 효과가 발현될 수 있음을 밝혔다.

주요어 : 거시양자상태, 원자계, 광학계

학번 : 2009-20391